Please cite this article in press as: De Kreijger et al., From photons to reactions: key concepts in photoredox catalysis, Chem Catalysis (2024), https://doi.org/10.1016/j.checat.2024.101110

Chem Catalysis

CellPress

Review

From photons to reactions: key concepts in photoredox catalysis

Simon De Kreijger,[1,3] Felix Glaser,[1,3] and Ludovic Troian-Gautier[1,2,*]
[1]UCLouvain, Institut de la Matière Condensée et des Nanosciences (IMCN), Molecular Chemistry, Materials and Catalysis (MOST), Place Louis Pasteur 1/L4.01.01, B–1348, Louvain-la-Neuve, Belgium
[2]Wel Research Institute, Avenue Pasteur 6, 1300 Wavre, Belgium
[3]These authors contributed equally
*Correspondence: ludovic.troian@uclouvain.be
https://doi.org/10.1016/j.checat.2024.101110

THE BIGGER PICTURE Photoredox catalysis is nowadays considered evident and represents a field that is under significant investigation. Using photons to drive chemical reactions is a fascinating endeavor that has led to numerous fundamental and industrial developments. However, although the tremendous output dedicated to photoredox catalysis speaks of fantastic development, the research community is also conscious that there is a need for more standardized methods to improve the development of light-induced transformations. This review does not seek to address the need for standardized methods but rather presents an original and conceptual approach to investigate, understand, and develop photoredox transformation based on key physical parameters of the photosensitizer, quencher, and solution. Understanding the foundation of light-induced processes will undoubtedly lead to robust and reproducible development and discoveries in this active field.

SUMMARY

Photoredox catalysis has emerged as a powerful tool for organic synthesis, enabling the generation of reactive intermediates under mild reaction conditions. In this review, a special emphasis is placed on key concepts essential to understand and subsequently optimize photoredox catalytic processes. These focus on the formation and deactivation of the excited state and its reactivity. Specifically, the importance of the excited-state lifetime for diffusional quenching, the formation of the encounter complex, and the crucial role of non-covalent interactions in facilitating pre-association between reagents are discussed. Furthermore, excited-state deactivation pathways induced by a quencher are considered, differentiating between energy-transfer and electron-transfer processes. Finally, we address the importance of cage escape yields for the case of electron-transfer quenching and the determination of reaction quantum yield by actinometry measurements. Comprehension of these parameters will enable the development of more efficient and selective photocatalytic processes and open technological locks.

INTRODUCTION

Organic chemistry has revolutionized our society through the virtually infinite number of transformations that can be imagined and conceived by researchers that have pioneered the field and those joining the field with fresh perspectives.[1–13] Organic chemistry has led to the development of molecules that are used in therapeutics and medicine, agriculture, packaging, the food industry, and many other fields. Historical developments coupled to tragic examples, such as thalidomide,[14,15] have led to a greater understanding of structure-property relationships and the further development of more selective drugs. However, despite the tremendous progress afforded by organic chemistry, the current environmental trend can point toward certain limitations of organic chemistry, such as reactions operating at high temperature, in harsh conditions, using high catalyst loading, or in the presence of quantitative additives such as oxidant or reductant. In addition, the use of toxic reagents and certain categories of solvent also represent a risk for the user and the environment if not handled or disposed of properly. These aspects are not necessarily detrimental to the development of organic chemistry but are merely avenues that scientists have tried to tackle, especially since the advent of "green chemistry."[16]

"Would it not be advantageous to make better use of radiant energy?"[17] Through these wise words, Giacomo Ciamician pioneered what is nowadays considered to be accepted; i.e., to use

Please cite this article in press as: De Kreijger et al., From photons to reactions: key concepts in photoredox catalysis, Chem Catalysis (2024), https://doi.org/10.1016/j.checat.2024.101110

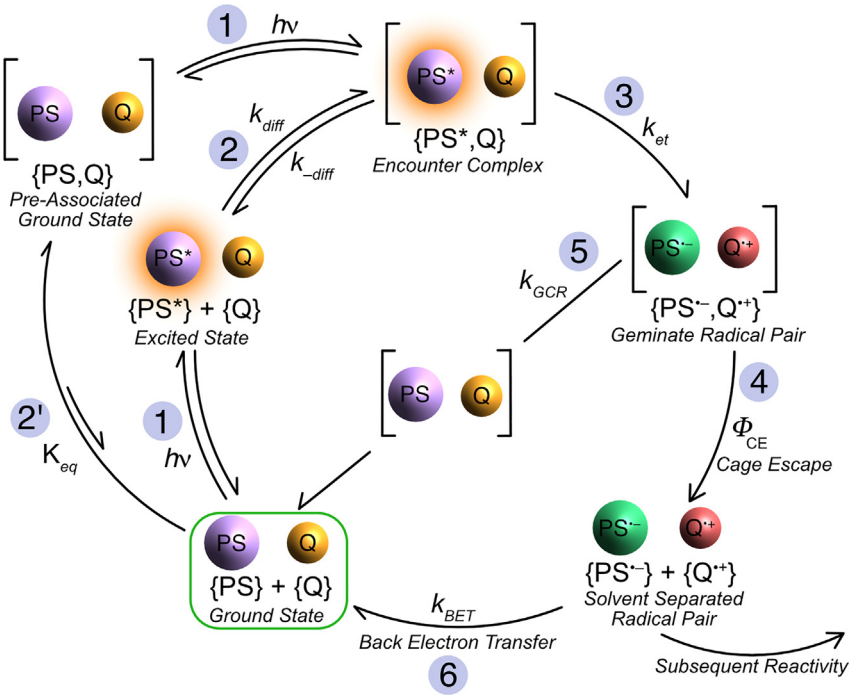

Figure 1. Photophysical and photochemical scheme describing the elementary steps between a photosensitizer (PS) and a quencher (Q) under light irradiation

The scheme is described for reductive excited-state quenching. The scheme is separated according to steps that are further described in the present review: (1) light absorption, excited-state population, and excited-state lifetime; (2) formation of the encounter complex via diffusion in the excited state or (2′) via pre-association in the ground state; (3) electron transfer; (4) cage escape (including cage escape yields); (5) geminate charge recombination; and (6) back electron transfer. These steps are associated with the corresponding rate constants for diffusional encounters (k_{diff}), electron transfer (k_{et}), geminate charge recombination (k_{GCR}), and back-electron transfer (k_{BET}). Note that step 3 could also operate via energy transfer, in which case the excited photosensitizer transfers energy to an energy acceptor and decays to the ground state. In that case, the notion of cage escape and geminate charge recombination become irrelevant.

light to drive chemical transformations. At the beginning of the 20th century, Ciamician and Silber used prolonged exposure to sunlight to perform transformations, such as the conversion of carvone to carvone camphor over several months. These transformations occurred using the UV part of the solar spectrum. It was decades later that Kellogg used $[Ru(bpy)_3]^{2+}$ as photocatalyst, where bpy is 2,2′-bipyridine, to investigate the light-induced reduction of sulfonium ions to the corresponding alkanes and thioethers.[18,19] Since then many different photocatalytic transformations were developed making use of a multitude of different photosensitizers.

Due to its unique operating principle, photoredox catalysis has several advantages: (1) it can be used to shorten the reaction time necessary for the synthesis of active compounds; (2) it allows the triggering of reactions at room temperature with visible light, therefore bypassing the need for harsh conditions; (3) the photosensitizer can selectively be activated with irradiation (i.e., the photosensitizers are not performing chemistry in the ground state); and (4) they are typically used in catalytic conditions to perform, most often, oxidation or reduction reactions. However, if not designed properly, these transformations still require the need of large excess of sacrificial electron donor (ED) or electron acceptor (EA).[20] Photoredox catalysis has already found applications at the industrial level, where it is, for example, used in the pharmaceutical industry for the optimization of [2 + 2] cycloaddition reactions[21] or to optimize the photoisomerization of an intermediate of vitamin D_2.[22] Moreover, photocatalysis in flow is used for a broad range of different chemical transformations that includes C–H arylation of arenes,[23] trifluoromethylation of ketones,[24] benzylic brominations,[25] and fluorinations.[26] Photosensitizers are also able to activate $^3O_2$ into $^1O_2$ via energy transfer (*vide infra*) and can be used to perform chemical oxidation, which are also performed at the industrial scale for the production of rose oxide developed by the company Symrise or for the photooxygenation of dihydroartemisinic acid in the synthesis of artemisinin implemented by Sanofi.[27–29]

Photoredox catalysis always relies on the premise that the photosensitizer reacts in its excited state with a quencher, i.e., a molecular entity that deactivates the photosensitizer's excited state either by energy transfer, electron transfer, or by other quenching processes that can include proton transfer, influence of the intersystem crossing rate, or a change in radiative and non-radiative rate constants.[30] In several cases, this quencher is a sacrificial ED or EA that is used in large concentrations, which represents a severe limitation in terms of atom economy.[31] The quencher can also be a reagent that will be incorporated in the backbone of the final product, which could therefore help bypass the need for sacrificial reagents if the generated reactive intermediates are thermodynamically competent to react with the reduced or oxidized photosensitizer. Overall, it becomes apparent that the interaction between the photosensitizer and the quencher as well as the different deactivation pathways from the excited state represent a very important aspect of the overall photocatalysis.

The guiding mechanistic scheme that will be used throughout this perspective is described in Figure 1. This mechanism focuses mainly on the factors influencing the steps leading to excited-state electron or energy transfer and cage escape yields for redox processes, while the follow-up elementary steps of the intermediates after separation (termed "subsequent reactivity" in Figure 1) are less in focus.[32] Each step will be decorticated throughout this tutorial review to provide insightful considerations that can be used for the further development of photoredox catalysis and future discoveries.

Please cite this article in press as: De Kreijger et al., From photons to reactions: key concepts in photoredox catalysis, Chem Catalysis (2024), https://doi.org/10.1016/j.checat.2024.101110

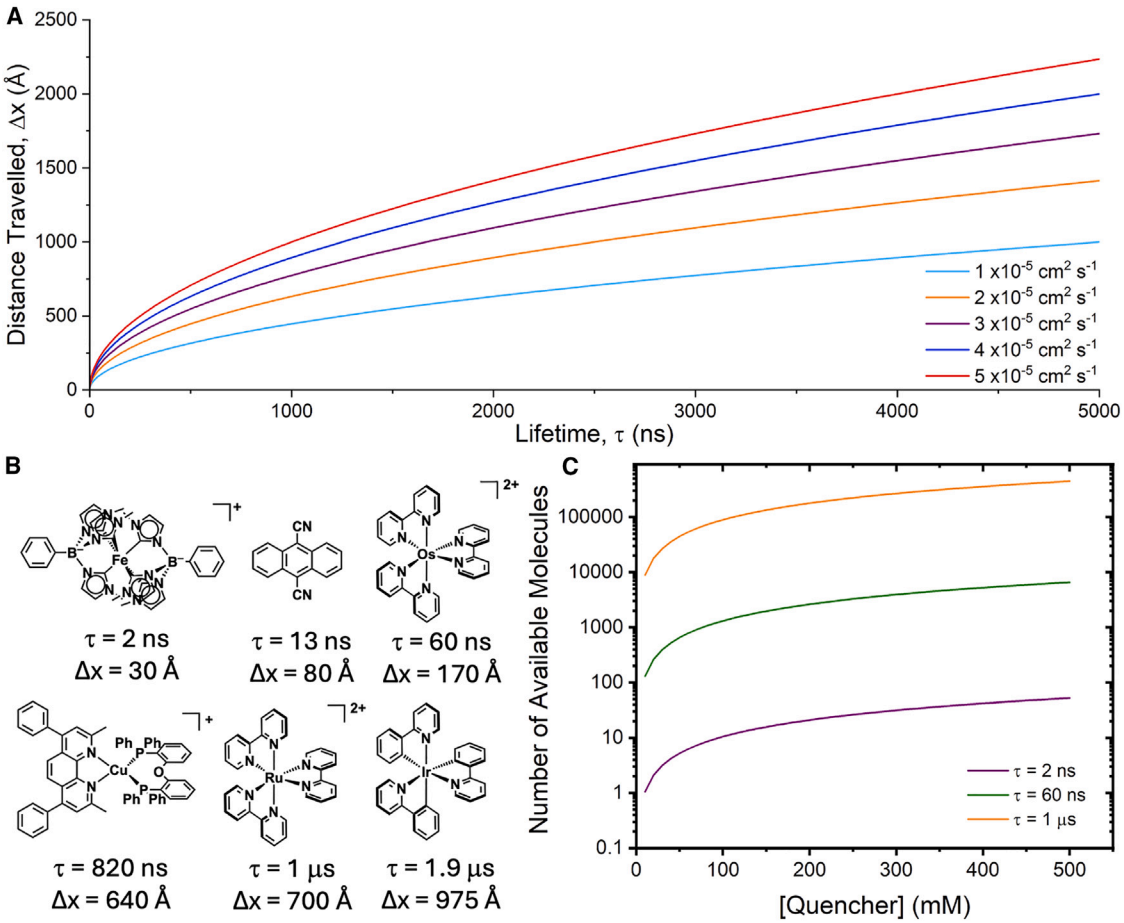

Figure 2. Lifetime and concentration effects on possible encounters

(A) Average distance traveled according to the excited-state lifetime of the indicated photosensitizer using Equation 1 with diffusion coefficients that ranged from 1 to 5 × 10^{-5} cm^2 s^{-1}.

(B) Structure of representative photosensitizers alongside their excited-state lifetime (τ) and distance traveled (Δx) assuming a diffusion coefficient of 2.5 × 10^{-5} cm^2 s^{-1} (acetonitrile).[33]

(C) Number of quencher molecules encompassed within the volume that an excited state can potentially travel through assuming a diffusion coefficient of 2.5 × 10^{-5} cm^2 s^{-1}.

EXCITED-STATE LIFETIME: ITS IMPORTANCE FOR DIFFUSIONAL QUENCHING

In diffusional bimolecular reactivity, the excited-state lifetime τ is probably the most critical parameter to consider. The excited-state lifetime is solvent dependent and sometimes concentration dependent, and, as such, it is necessary to measure the excited-state lifetime of the photosensitizers in controlled conditions. Importantly, τ controls the distance that an excited state is able to travel before undergoing deactivation. Thus, excited-state lifetimes play a crucial role in the quenching efficiency. The Einstein equation can be used to determine an average distance (Δ*x*) that an excited molecule can travel within its lifetime for a solvent-dependent diffusion coefficient *D* (Equation 1).[30]

$$\Delta x = \sqrt{2D\tau} \qquad \text{(Equation 1)}$$

The average distance that an excited state can travel as a function of the excited-state lifetime is given in Figure 2A, assuming diffusion coefficients that range from 1 to 5 × 10^{-5} cm^2 s^{-1}. In this example, it is straightforward to understand why Ru(II) and Ir(III) photosensitizers with microsecond excited-state lifetimes have encountered their success in photoredox catalysis. Indeed, a photosensitizer such as $[Ru(bpy)_3]^{2+}$ with an excited-state lifetime of 1 μs is able to travel on average 700 Å in acetonitrile,[33] assuming a diffusion coefficient of 2.5 × 10^{-5} cm^2 s^{-1}. Under similar conditions, a photosensitizer with an excited-state lifetime of 2 ns, such as the Fe(III) photosensitizer depicted in Figure 2, would only be capable of traveling over a distance of ~30 Å, thus limiting the number of potential encounters with a quencher. Fluorescent organic photosensitizers, such as 9,10-dicyanoanthracene (DCA), with a singlet excited-state lifetime of 13 ns, is thus capable of traveling an average distance of

Please cite this article in press as: De Kreijger et al., From photons to reactions: key concepts in photoredox catalysis, Chem Catalysis (2024), https://doi.org/10.1016/j.checat.2024.101110

80 Å, again assuming a diffusion coefficient of 2.5 × 10^{-5} cm^2 s^{-1}.

The number of quencher molecules contained within the average volume that an excited photosensitizer can potentially travel through can be crudely estimated assuming an even distribution of quencher molecules at a fixed concentration within the solution. As highlighted earlier, excited $[Ru(bpy)_3]^{2+}$ can diffuse over an average distance of 700 Å in acetonitrile (assuming D = 2.5 × 10^{-5} cm^2 s^{-1}).[33] Taking this distance as the maximal radius of a sphere, the corresponding theoretical volume that the excited photosensitizer could potentially explore can be determined. Finally, the number of quencher molecules within that sphere can also be roughly estimated based on Avogadro's number and the concentration of an equally distributed quencher. For the case of $[Ru(bpy)_3]^{2+}$ the excited complex can potentially diffuse in a volume of 1.44 × 10^{-21} m^3 (1.44 × 10^6 nm^3) and encounter potentially 865 quencher molecules for the case of a 1 mM quencher solution (with consequently 6.022 × 10^{23} molecules m^{-3}). Unsurprisingly, for an iron sensitizer with an excited-state lifetime of 2 ns, the number of encounters decreases drastically and a concentration of 10 mM is needed to statistically have 1 encounter. A concentration of 250 mM would lead to 26 potential encounters. These theoretical considerations clearly highlight the importance of the excited-state lifetime of the photosensitizer as one key parameter for efficient catalysis and reasonable long lifetimes are needed to allow efficient diffusional excited-state quenching. This aspect will be further developed in the appropriate section but assuming a diffusional quenching rate constant of 10^{10} $M^{-1}s^{-1}$ and a concentration of quencher of 10 mM, then a photosensitizer with a 2-ns excited-state lifetime would only be quenched by 2%, whereas this quenching efficiency would increase to over 90% if the photosensitizer exhibits an excited-state lifetime of 1 μs (*vide infra*). In addition, it should be emphasized that not all encounters induce excited-state deactivation, as discussed later in this perspective.

Bimolecular reactivity of the photosensitizer in the excited state proceeds via the formation of an encounter complex that is formed upon the collision of the photosensitizer and the quencher (step 2 in Figure 1). In some instances, the encounter complex can be formed in the ground state via pre-association of the photosensitizer and the quencher, thereby suppressing the need for diffusional collisions and making the ground state equilibrium K_{eq} an elemental step to form the photoactive intermediate (step 2′ in Figure 1, *vide infra*). Thus, for species diffusing in solution, the formation of the encounter complex is controlled by a rate constant for diffusion (k_{diff}). Within this encounter complex, electron transfer occurs by a first-order reaction with units of s^{-1}. As the units of the association equilibrium K_A are M^{-1}, the product of K_A and the rate constant of electron transfer k_{et} is referred to as the activated rate constant ($M^{-1}s^{-1}$) as described further by Sutin, where k_q is the quenching rate constant (*vide infra*, Equation 2).[34] Further information about these diffusion processes has been extensively reported.[34–38]

$$\frac{1}{k_q} = \frac{1}{k_{diff}} + \frac{1}{K_A k_{et}} \qquad \text{(Equation 2)}$$

PRE-ASSOCIATION OF THE ENCOUNTER COMPLEX

An alternative approach to circumvent the limitations set by diffusion, especially for photosensitizers with short excited-state lifetimes, is to pre-associate the photosensitizer and the quencher in the ground state (step 2′ in Figure 1). Such pre-association can lead to rapid excited-state quenching that occurs subsequently to the population of the excited state without the need for diffusional encounters within the lifetime of the photoactive compound. This general quenching mechanism is often called "static" to emphasize that it does not rely on diffusion. In contrast to diffusional excited-state quenching, the photoactive species in this case is not the photosensitizer itself but rather the (ground-state) encounter complex. In general, three different cases relying on pre-association are considered herein: (1) bond dissociation of a coordinated ligand in metal complexes via ligand-to-metal charge transfer excitation, (2) donor-acceptor interactions to form a new photoactive intermediate prior to excitation, and (3) non-covalent interactions in the ground state. Ideally, these ground-state interactions also cause spectroscopic changes and can therefore often be identified and characterized by UV-visible absorption or NMR spectroscopy.[39] Pre-association between a photosensitizer and a quencher can occur through either coordination bonding[40,41] or non-covalent interactions, including Coulombic/ionic interactions,[42] hydrogen bonding,[43,44] and π-π stacking.[45] Subsequent sections will discuss the applications of these concepts based on selected examples from the literature.

Recently, a strategy involving the population of ligand-to-metal charge transfer (LMCT) excited states of metal complexes received some attention to generate highly reactive radical intermediates relevant to organic transformations via homolytic metal-ligand bond cleavage.[46,47] These LMCT states arise from an electronic transition, where, upon excitation, a ligand-based filled orbital donates an electron to an empty or partially filled metal-centered orbital (Figure 3). These states are typical in complexes bearing electrophilic, high-valent metal center within the 3d block, such as Fe(III), Cu(II), or Ti(IV). Conversely, as the ligand serves as the internal electron source in these transitions, the presence of electron-rich σ or σ + π donor ligands such as halides, carboxylates, or azide are favorable for the occurrence of the LMCT transition at reasonably low energies (i.e., with absorption bands close to the visible part of the electromagnetic spectrum). Under light irradiation, LMCT transitions involve the population of an anti-bonding orbital, leading to decreased bond order in the M–L bond, consequently making them more labile and facilitating their cleavage. This occurrence of fast non-radiative deactivation via bond dissociation results in non-emissive excited states. Consequently, these excited states are not detectable via steady-state photoluminescence spectroscopy and are usually characterized by ultrafast transient absorption spectroscopy.[48] In terms of reactivity, LMCT states facilitate the transformation of nucleophilic entities into open-shell species through coordination to a metal center and subsequent photoexcitation, often resulting in homolytic cleavage of M–L bonds within these complexes and formation of a reduced metal complex and a radical product (Figure 3).[46,49]

Please cite this article in press as: De Kreijger et al., From photons to reactions: key concepts in photoredox catalysis, Chem Catalysis (2024), https://doi.org/10.1016/j.checat.2024.101110

CellPress

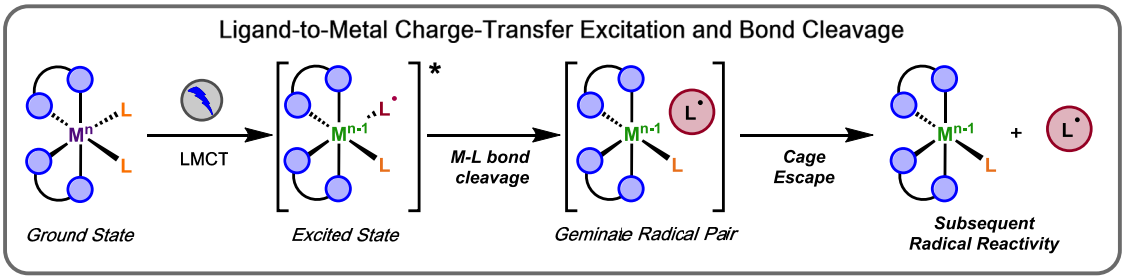

Figure 3. General photochemical processes via ligand coordination and light-induced homolytic cleavage by a ligand-to-metal charge-transfer excitation

Based on previous research investigating the halogen photoelimination from Ni(III) complexes assisted by the secondary coordination sphere,[50,51] Nocera and coworkers investigated the trajectory of a chlorine radical released from an Fe(III) pyridinediimine (PDI) complex upon photoexcitation.[52] This work highlighted the formation of a Cl˙|arene adduct within the geminate radical pair that helps directing its subsequent activity toward specific C–H bonds of a substrate molecule. Inspired by this finding, they investigated the use of Cl˙|arene interaction to confine photoeliminated chlorine radicals within the secondary coordination sphere, offering control over their reactivity. To this aim, a series of Fe(III) PDI complexes incorporating different aromatic groups were designed.[48] These complexes exhibited steric selectivity, favoring the activation of more accessible C–H bonds over weaker C–H bonds in chlorine-radical-mediated C–H bonds functionalization reactions. Femtosecond-resolved transient absorption measurements indicated that one process involved the rapid recombination of Fe(II) with Cl˙ that does not form an adduct, while a slower process was attributed to the Cl˙|arene adduct formation (τ = 70 ps). Therefore, this longer-lived species is primed to engage in reactions with substrate molecules proximate to the complex. Photochlorination of 3-methylpentane with this iron photoredox catalysis exhibited higher selectivity for more accessible 1° and 2° C–H bonds over weaker 3° C–H bonds. This procedure was then applied to a larger scope of substrates and exhibited the same selectivity for 1° and 2° C–H bonds. Next to this specific example, several applications of LMCT-induced M–L homolytic cleavage were recently investigated for synthetic transformations mediated by Fe(III),[40,53–55] Cu(II),[56–60] Ni(III),[41,61,62] Co(III),[63–65] and Ti(IV)[66–69] metal centers following a similar reactivity sequence, as described in Figure 3.

Recently, strategies based on ground state pre-association of an EA substrate (Lewis acid) and an ED substrate (Lewis base) to induce the formation of a new molecular entity called an electron donor-acceptor (EDA) complex have been recognized as a powerful strategy to broaden the scope of visible light-induced radical chemistry (Figure 4). While the acceptor (A) and donor (D) species may not absorb visible light, the physical properties of the resulting EDA complex differ from those of its constituent substrates due to the formation of new molecular orbitals. This results from the interaction between the frontiers orbitals of the highest occupied molecular orbital (HOMO) of the donor and the lowest unoccupied molecular orbital (LUMO) of the acceptor (Figure 4B).[70] The newly formed chemical entity exhibits a distinctive absorption band, known as the charge transfer band, corresponding to an electronic transition between the ground and excited states. Upon excitation, the excited state of the EDA complex is populated, typically involving an intramolecular charge transfer of an electron from the donor to the acceptor, resulting in the formation of a geminate radical ion pair characterized by a net charge separation on two different molecules (Figure 4A). Initially, the application of EDA complex photochemistry in chemical synthesis was limited.[71] This limitation likely stemmed from the challenge of preventing unproductive geminate charge recombination from the generated radical ion pair, which would revert the EDA complex to its ground state (Figure 4A). To address this challenge and convert EDA complex activation into a productive synthetic strategy, one approach involves incorporating a suitable leaving group (LG) into one of the reaction partners (Figure 4A). This leaving group is likely to induce an irreversible fragmentation event that competes with geminate charge recombination. Consequently, upon cleavage of the leaving group, reactive radical intermediates capable of initiating synthetically valuable transformations are generated.[72–74] Over the past decades, the photochemistry of EDA complexes has been extensively developed and applied to different synthetic strategies such as the direct coupling between the donor and the acceptor substrates[75–77] by using sacrificial donors and redox auxiliaries,[78–82] as well as in organocatalysis and asymmetric photochemical processes.[83–85] A significant step forward in this field was opened when catalytic rather than stoichiometric amounts of donor or acceptor were introduced and catalytic applications became accessible. This has been shown for alkylation radical reactions using a combination of triphenylphosphine and sodium iodide,[86] aminodecarboxylation of tetrachlorophthalamide esters,[87] monofluoromethylation of *N*-arylacrylamides,[88] and many other chemical transformations.[89–97] Nevertheless, in many cases, catalyst loadings of at least 10% are needed to achieve reasonable changes in the absorption and/or electrochemical properties to allow the formation of new photoactive intermediates.[98]

The processes discussed up to now were mostly focused on the formation of novel photoactive species with labile leaving groups or donor acceptor complexes. Non-covalent interactions between a photosensitizer and a quencher also offer interesting alternatives that can lead to altered photophysical properties through the formation of a pre-associated encounter complex

Please cite this article in press as: De Kreijger et al., From photons to reactions: key concepts in photoredox catalysis, Chem Catalysis (2024), https://doi.org/10.1016/j.checat.2024.101110

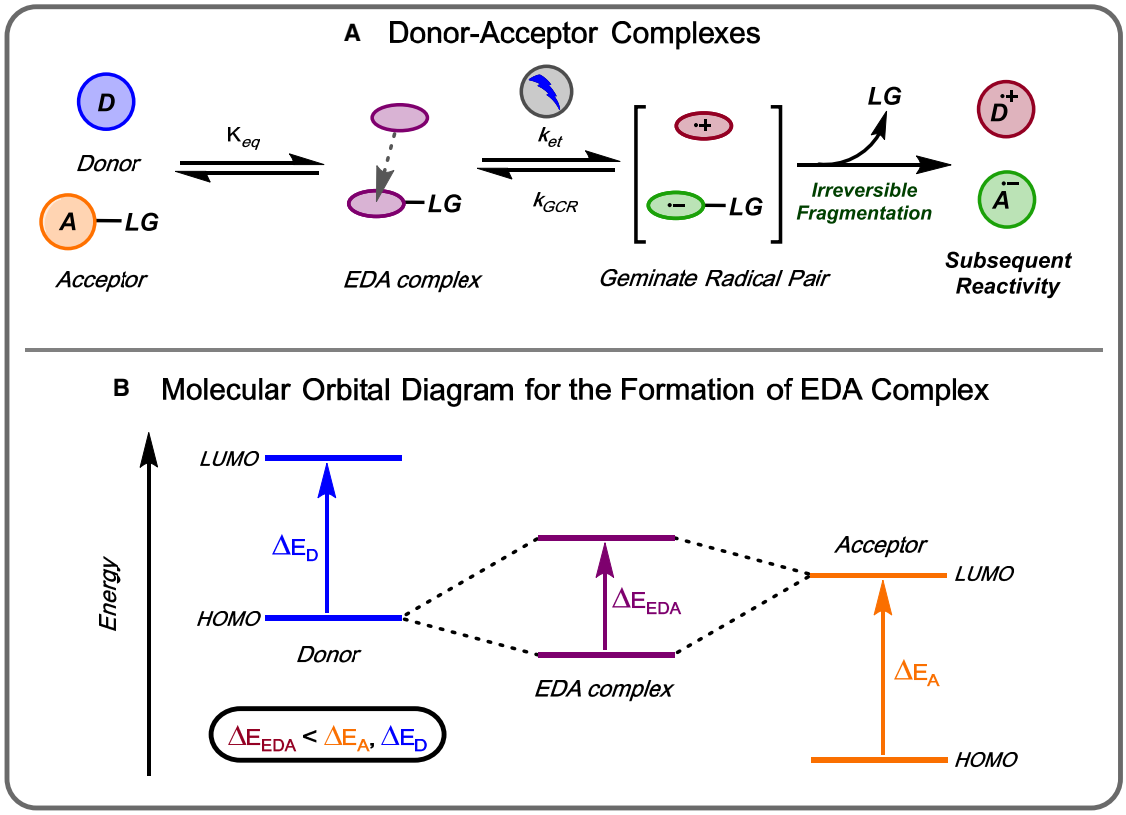

Figure 4. General concept of EDA reactivity

(A) General photochemical processes via the formation of electron donor-acceptor (EDA) complexes with association constant for the formation of the EDA complex (K_{eq}). The donor or the acceptor bears in most cases a leaving group (LG) to induce an irreversible fragmentation.

(B) Molecular orbital diagram for the formation of EDA complex by interactions between the frontier orbitals of the HOMO of the donor and the LUMO of the acceptor.

that will experience changes in reactivity compared to the parent photosensitizer (Figure 5).

For example, Jiménez and coworkers investigated non-covalent interactions between a metal complex and a substrate by hydrogen bonding interactions with a short-lived iron photocatalyst. The group reported the excited-state reactivity of a heteroleptic iron(III) complex ($[Fe^{III}(pzTP)(CN)_3]^-$) bearing three monodentate cyanides and a tridentate tetrakis(pyrazolyl)borate ligand (pzTP).[99] Its reactivity toward a benzylic alcohol was found to be enhanced by pre-association of the photosensitizer and the substrate though hydrogen-bonding interactions. The detected excited-state lifetime of 80 ps obtained for the red-emitting complex is too short for diffusional encounters (as highlighted in the previous section). Despite its brevity, $[Fe^{III}(pzTP)(CN)_3]^{-*}$ displays a very attractive excited-state redox potential of $E_{1/2}(Fe^{*III/II})$ = 2.31 V vs. NHE. Note that the asterisk is used to describe the excited-state nature of the photosensitizer or the excited-state redox potentials. This points toward its strong promise as a photo-oxidant regardless of its limited distance coverage of 5.6 Å according to Equation 1. The excited-state reactivity of this photosensitizer was investigated toward the photo-oxidation of alcohols as challenging model substrates. Irradiating a solution containing $[Fe^{III}(pzTP)(CN)_3]^-$ and benzyl alcohol with a blue light-emitting diode (LED) (λ_{exc} = 440 nm) led to the formation of benzaldehyde from a net 2 e^- oxidation in 92% yield within 3 h of irradiation. While this result confirmed the effective photo-oxidation reactivity, the short excited-state lifetime suggested the involvement of pre-association interactions with the substrate. This aspect was investigated spectroscopically by the addition of alcohol substrates to a solution containing $[Fe^{III}(pzTP)(CN)_3]^-$, which resulted in a slight redshift in one of the LMCT bands, pointing toward weak interactions between the cyanide and the alcohol influencing the coordination sphere of the iron center. This observation was further supported by the corresponding IR spectrum, revealing a significant shift in the C–N stretching peak toward higher energy in the presence of substrate. This interaction was consistent with hydrogen bonding between the CN ligand and the alcohol group. In conclusion, a crucial role was attributed to hydrogen bonding in facilitating the reactivity of $[Fe^{III}(pzTP)(CN)_3]^-$ with the alcohol substrate by pre-association between substrate and catalyst, thereby circumventing the limit set by the short excited-state lifetime.

In 2024, Kerzig and coworkers reported a new approach based on Coulombic interactions for mediator-enhanced sensitized triplet-triplet annihilation (TTA) upconversion in solution.[100] Sensitized TTA upconversion presents an enticing opportunity to convert two low-energy photons into a higher-energy photon by

Please cite this article in press as: De Kreijger et al., From photons to reactions: key concepts in photoredox catalysis, Chem Catalysis (2024), https://doi.org/10.1016/j.checat.2024.101110

utilizing both a light-harvesting triplet sensitizer and an annihilator to generate a fluorescent singlet state.[101–107] Typically, achieving efficient energy transfer requires high concentrations of annihilator, leading to undetectable emission due to inner filter effects caused by that large concentration. In their report, the group found that the upconversion quantum yields could be drastically increased through Coulombic interactions in dimethylformamide. In this case, the dicationic photosensitizer $[Ru(phen)_3]^{2+}$, where phen is 1,10-phenanthroline, could undergo Coulombic interactions with a monoanionic pyrene-1-sulfonate (PMS) mediator in the presence of a neutral 9,10-diphenylanthracene (DPA) annihilator. Overall, the mediator enhances the triplet energy transfer from the photosensitizer to the annihilator via a cascade process. Bimolecular energy transfer rate constants of 9.1×10^9 M^{-1} s^{-1} and 2.0×10^9 M^{-1} s^{-1} were determined for the energy transfer from $[Ru(phen)_3]^{2+}$ to PMS and DPA, respectively. To further understand the role of ionic interactions, unsubstituted pyrene was used as an uncharged reference energy acceptor. The determined rate constant with this unsubstituted pyrene was 1.4×10^9 M^{-1} s^{-1}, indicating that the energy-transfer process to the unsubstituted pyrene was nearly one order of magnitude slower compared to the sulfonated analogue. Nevertheless, the static contribution for the energy transfer from the photosensitizer to the mediator induced by Coulombic interaction had only minor contributions to the global quenching process (<10%). These findings indicate that ionic interactions by charged photosensitizer and quencher can also enhance a diffusional quenching step. Interestingly, when the monoanionic pyrene mediator was replaced by a tetraanionic derivative (pyrene-1,3,6,8-tetrasulfonate (PTS)) in water, static contributions were drastically increased to almost 90% of the overall quenching process.[108] This enhancement of the energy transfer step allowed efficient energy transfer even with low concentrations (120 μM) of PTS. This system was efficiently used to produce singlet oxygen in air-saturated water and applied for the synthesis of 5-hydroxy-5-(hydroxymethyl)-furan-2(5H)one, where 93% yield were obtained after 5 h of green light irradiation. Under similar conditions, the thioanisole photooxygenation to methyl phenyl sulfoxide also proceeded with yields greater than 90% in 1 h. Next to these examples based on singlet oxygen generation by an energy transfer cascade, reductive quenching with ascorbate as sacrificial ED was investigated in the presence and absence of PTS. Significantly higher cage escape yields for the quenching of ^{3}*PTS ($\Phi_{CE} \sim 1$) were found compared to a direct excited-state electron transfer to the ruthenium-based photocatalyst that operated with $\Phi_{CE} = 0.21$. Overall, this superior electron transfer efficiency of the Coulombic dyad was also reflected in the reductive dehalogenation of 2-bromopyrazine, where reaction yields of 94% were obtained after 3 h of green light irradiation. The reference measurement without PTS present only provided 16% of product under the same reaction conditions. Pinacol coupling reactions of fluorinated benzaldehyde derivatives as a different class of reactions also proceeded with reaction yields greater than 70% for the mediated system. Note that a more extensive discussion of cage escape yields for excited-state quenching by electron transfer is provided later within this review.

In addition to these Coulombic interactions, noncovalent π-π interactions of a photosensitizer and a catalyst also offer an advantage by providing dynamic interactions that involve weak and/or reversible intermolecular attractions, allowing both connection and dissociation to occur during photocatalysis. While enhancing intermolecular electron transfer, dynamic interactions can also prevent irreversible dissociation between the PS and the catalyst, which is hardly applicable within systems based on covalent bonds.[44] Ouyang and coworkers recently designed a new system fully based on Earth-abundant elements taking advantage of π-π interactions between a pyrene-decorated phenanthroline Cu(I) photosensitizer and a pyrene-appended Co(II) catalyst for light-driven CO_2 to CO reduction.[109] Interestingly, introducing the pyrene moiety on the Cu(I) photosensitizer ($[Cu^I(xantphos)(pybcp]^+$) led to a dual emission behavior and a decrease in the emission lifetime for the MLCT emission (9 ns) compared to the prototypical $[Cu^I(xantphos)(bcp)]^+$ (289 ns, bcp = bathocuproine). ^{1}H NMR titration was employed to assess the binding affinity between the Cu(I) PS and Co(II) co-catalysts as well as their respective self-interaction trends. These experiments demonstrated larger binding constants for Co(II)–Cu(I) (207 M^{-1}) than for Co(II)–Co(II) (132 M^{-1}) and Cu(I)–Cu(I) (50 M^{-1}). The binding constant between Co(II) and Cu(I) was in the same order of magnitude as the one reported between Co(II) and a pyrene-decorated Ir(III) photosensitizer (199 M^{-1}),[109] consistent with the reversible/dynamic nature of these interactions. Photocatalytic CO_2 reduction experiments were then investigated by pairwise comparison of the different combinations of pyrene-decorated and undecorated catalysts in acetonitrile solution. Under reaction conditions with suitable ED and proton sources, the combination of 100 μM of the Co(II) catalyst and 100 μM of the $[Cu^I(xantphos)(pybcp]^+$ PS demonstrated the highest turnover number (338), turnover frequency (264 h^{-1}), selectivity (97%), and quantum yield (19%), indicative of the promoting effect of the π-π interactions.

Overall, the specific examples discussed in this section highlight the utility of the formation of a pre-associated species prior to photoexcitation to form new photoactive intermediates and circumvent the drawbacks of short excited-state lifetimes, which can also induce new reactivities (e.g., for donor-acceptor complexes) or enhanced selectivity.

EXCITED-STATE REACTION AND MECHANISM: ENERGY TRANSFER VS. ELECTRON TRANSFER

As previously stated, the excited-state lifetime of a photosensitizer has a significant impact on the number of potential encounters with different quenchers in solution (Figure 2). The kinetic processes of excited-state quenching in diffusional and/or static elementary steps represent an important aspect of photocatalysis. Unsurprisingly, the number of encounters is not only dependent on the excited-state lifetime but also depends on the nature of the solvent and the concentration of quencher.[33] In fact, the diffusion-limited rate constant can be significantly different depending on the solvent. For example, acetonitrile, a commonly used polar solvent, has a diffusion-controlled rate constant for bimolecular encounters that is about six times that determined in dimethyl sulfoxide ($k_{diff} = 1.9 \times 10^{10}$ $M^{-1}s^{-1}$ vs. 3.3×10^9 $M^{-1}s^{-1}$).[33]

Please cite this article in press as: De Kreijger et al., From photons to reactions: key concepts in photoredox catalysis, Chem Catalysis (2024), https://doi.org/10.1016/j.checat.2024.101110

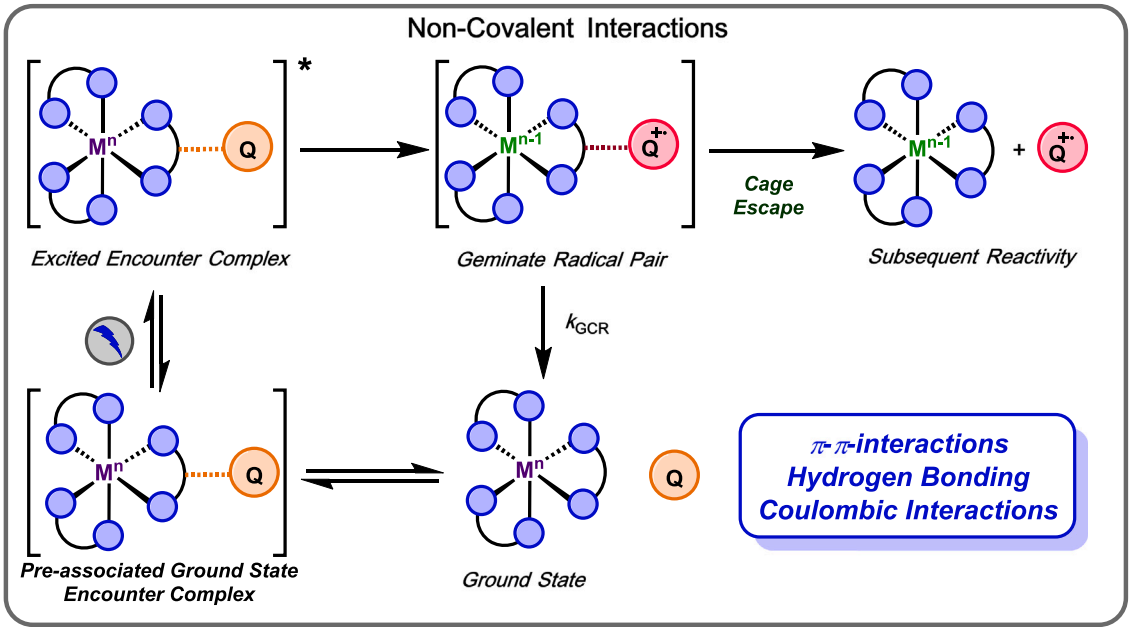

Figure 5. General photochemical processes via ground state pre-association by non-covalent interactions between a photosensitizer and a quencher

According to the International Union of Pure and Applied Chemistry (IUPAC), a quencher is a molecular entity that deactivates (quenches) an excited state of another molecular entity, either by energy transfer, electron transfer, or by a chemical mechanism.[110] The excited-state quenching is often determined through the time-honored model described by Otto Stern and Max Volmer where the steady-state or time-resolved photoluminescence intensity of a photosensitizer is measured as a function of the quencher concentration.[30,111,112] A first-order dependence on the quencher concentration ([Q]) allows the Stern-Volmer constant (K_{sv}) to be determined, the reciprocal of which is equal to the quencher concentration necessary to quench half of the excited photosensitizers. The quenching rate constant (k_q) can then be determined by dividing K_{sv} by the excited-state lifetime in the absence of quencher (τ_0). For steady-state measurements, the unquenched photoluminescence intensity (PLI_0) is divided by the emission intensity in the presence of the quencher (PLI). In both cases the well-known Stern-Volmer relationship correlates the observed rate constant (k_{obs}) and the rate constant (k_0—an intrinsic property of the photosensitizer in the respective conditions—and can thus be written as Equation 3.

$$\frac{k_{obs}}{k_0} = \frac{PLI_0}{PLI} = \frac{\tau_0}{\tau} = 1 + K_{SV}\cdot[Q] = 1 + k_q\cdot\tau_0\cdot[Q] \quad \text{(Equation 3)}$$

The quenching efficiency η for the electron transfer pathway in relation to all other excited-state deactivation pathways can be extrapolated using the previously determined parameters through Equation 4.

$$\eta = \frac{K_{SV}\cdot[Q]}{1+K_{SV}\cdot[Q]} = \frac{k_q\cdot[Q]}{k_0+k_q\cdot[Q]} \quad \text{(Equation 4)}$$

Thus, the quenching efficiency depends on the excited-state lifetime ($\tau_0 = {k_0}^{-1}$), the concentration of quencher ([Q]), and the quenching rate constant k_q. A visual example is given in Figure 6 for quenching rate constants of 1×10^{10} $M^{-1}s^{-1}$ and 5×10^9 $M^{-1}s^{-1}$ over a concentration range between 0 and 100 mM and excited-state lifetimes that range from 0.1 ns to 10 μs.

Even if the reaction is diffusion controlled with large quenching rate constants, the quenching efficiency can be very small if the excited-state lifetime is smaller than 1 ns (pale blue trace in Figure 6). This is why photosensitizers with sub-nanosecond excited-state lifetime are often considered inoperable for bimolecular reactivity, unless ground-state association occurs as discussed in the previous section. Similarly, photosensitizers with short excited-state lifetime (2–5 ns) often require large concentration of quencher and high bimolecular quenching rate constants to proceed efficiently, whereas much smaller concentrations than those typically used in the literature could be sufficient for photosensitizers with excited-state lifetimes upwards of 100 ns (Figure 6). In fact, for reasonably long excited-state lifetimes (>10 μs), even efficient quenching can be achieved with rate constants significantly below the diffusion limit in the respective solvent. On the other hand, for bimolecular quenching rate constants that are too small, i.e., typically several orders below the diffusion limit, even high concentrations of quencher do not result in efficient excited-state deactivation. These considerations highlight the interplay between the excited-state lifetime τ_0, the quenching rate constant k_q, and the quencher concentration [Q].

Thus, it is not only the number of possible encounters at a given concentration of quencher that is relevant but also the ability of the quencher to introduce an additional deactivation

Please cite this article in press as: De Kreijger et al., From photons to reactions: key concepts in photoredox catalysis, Chem Catalysis (2024), https://doi.org/10.1016/j.checat.2024.101110

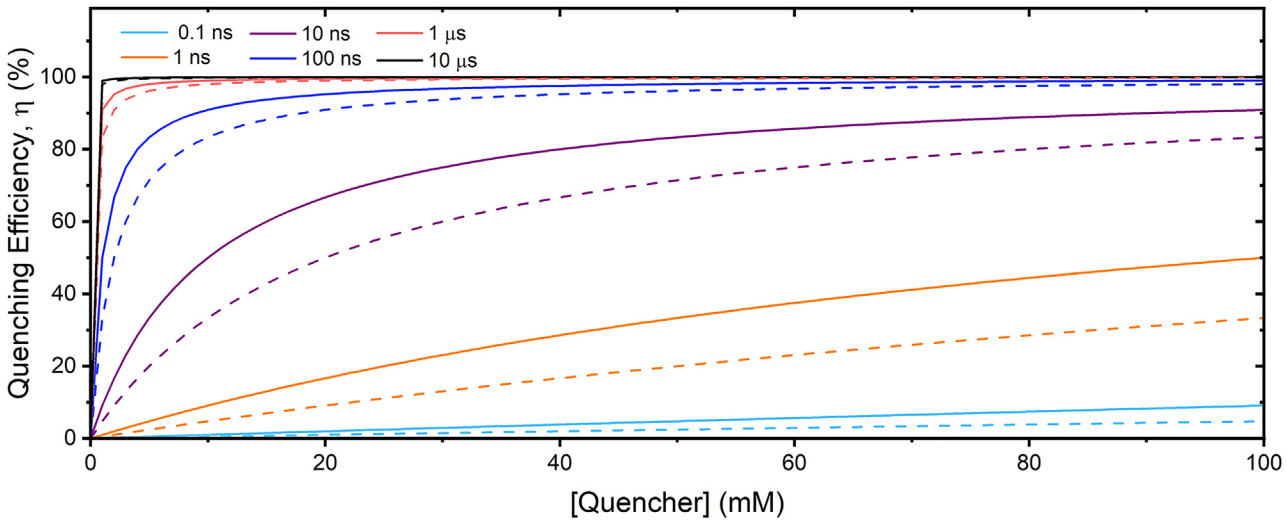

Figure 6. Quenching efficiency as a function of quencher concentration

The quenching efficiency was determined through Equation 4, using the indicated excited-state lifetime and quenching rate constants of 1×10^{10} $M^{-1}s^{-1}$ (solid) and 5×10^{9} $M^{-1}s^{-1}$ (dashed).

pathway that is quantified by the corresponding quenching rate constant (k_q). Importantly, the kinetic aspects discussed up to now should also be complemented by thermodynamic considerations in order to fully understand the excited-state quenching processes. These were only indirectly covered up to now. In addition, the nature of the excited-state deactivation pathway introduced by the quencher has not yet been covered as another fundamental aspect of excited-state quenching processes (i.e., if there is an energy or electron transfer occurring). Here, it is important to emphasize that Stern-Volmer analyses of the emission intensities or excited-state emission lifetimes (Equation 3) are not able to distinguish between energy or electron transfer as quenching pathways. To characterize the relevant processes, other complementary methods such as transient absorption spectroscopy are needed.[113,114] This has, for example, recently received some attention in studies on metallaphotoredox catalysis for light-driven cross-coupling reactions with nickel catalysts in combination with a photoactive co-catalyst. Depending on the properties of the photocatalyst and the reaction conditions, the overall mechanism can differ.[115–117]

Among the different excited-state quenching mechanisms, two main deactivation processes are often proposed: electron transfer or energy transfer. These two different processes can each be divided into an additional two subcategories, which will be individually discussed in the following subsection. For the case of excited-state quenching proceeding via energy transfer, Förster or Dexter mechanisms are differentiated for the energy transfer from an excited PS to an energy acceptor (EnA, Figure 7A). For excited-state quenching of the photosensitizer by electron transfer the two different pathways are oxidative or reductive electron transfer (Figure 7B).

A (Förster) resonance energy transfer (FRET; top part in Figure 7A) is dependent on the dipole-dipole interactions between the excited state of the energy donor (^{1}*PS) and a ground state of the EnA. An important feature for efficient Förster energy transfer includes a significant degree of spectral overlap between the emission of the energy donor and absorbance of the energy acceptor.[118] In addition, a marked distance dependence with r^{-6} for the FRET rate constant k_{FRET} is characteristic for this type of energy-transfer process. It is important to notice that FRET does not include any exchange of electrons between the donor and acceptor. This is a clear contrast to the second energy-transfer process discussed hereafter. Indeed, a Dexter energy transfer operates by a concerted electron exchange mechanism between the energy donor and the energy acceptor (bottom part in Figure 7A).[119] It is worth emphasizing that, in the case of energy transfer from a triplet excited state to a singlet ground state, this can only occur via Dexter energy transfer—and not via FRET—due to Wigner's spin conservation rule that states that the total electron-spin angular momentum of the transition partners should not change upon energy (or electron) transfer.[120,121] Thus, a triplet excited state can also undergo energy transfer with a triplet acceptor, such as ground-state $^3O_2$.[122] There have also been reports of energy transfer from triplet excited states to quartet ground states to generate a doublet excited state and the corresponding singlet ground state product and other mechanisms have been proposed as well.[123–125] As a consequence, for processes relying on sensitized energy transfer from triplet state, Dexter energy transfer is the relevant mechanistic process.[126–129] Energy transfer has received some attention in recent years for photocatalysis and as initial step for triplet-triplet annihilation upconversion with very good overview articles summarizing concepts and applications.[103,128,130–132]

As mentioned previously, excited-state quenching via electron transfer can operate according to two mechanisms: reductive or oxidative excited-state quenching.[133] In an oxidative quenching cycle, a suitable EA receives an electron from the excited photosensitizer, which yields a reduced EA and an oxidized photosensitizer (top part of Figure 7B). In contrast, with a suitable ED that is able to provide an electron to the excited photosensitizer, a

Please cite this article in press as: De Kreijger et al., From photons to reactions: key concepts in photoredox catalysis, Chem Catalysis (2024), https://doi.org/10.1016/j.checat.2024.101110

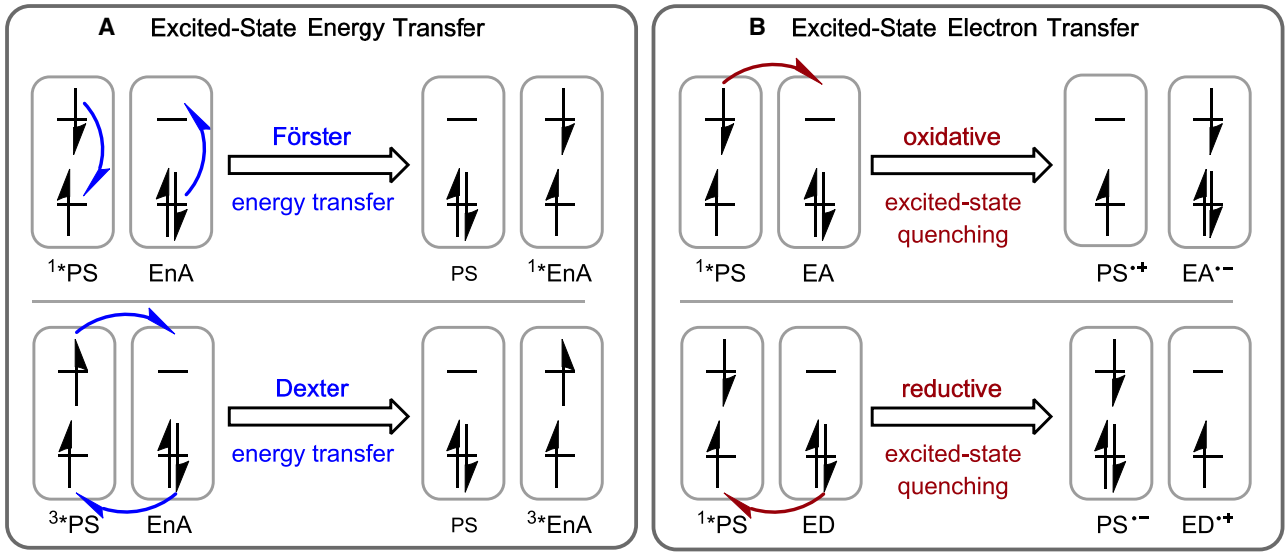

Figure 7. Excited-state quenching processes

Excited-state quenching of an excited photosensitizer (*PS) via (A) energy transfer to an energy acceptor (EnA) or (B) excited-state electron transfer to an EA or from an ED.

reductive quenching pathway is possible, which results in an oxidized ED and a reduced photosensitizer (bottom part of Figure 7B). Overall, the reduction or oxidation of the PS are facilitated in the excited state by the energy difference between the ground state and excited state (E_{00}). The excited-state oxidation or reduction potential can be estimated by the famous Rehm-Weller equations[134,135]:

$$E^*_{red} = E_{\frac{1}{2}}\left(PS^{*(n/(n-1))}\right) = E_{\frac{1}{2}}\left(PS^{(n/(n-1))}\right) + E_{00} \quad \text{(Equation 5)}$$

$$E^*_{ox} = E_{\frac{1}{2}}\left(PS^{*((n+1)/n)}\right) = E_{\frac{1}{2}}\left(PS^{((n+1)/n)}\right) - E_{00} \quad \text{(Equation 6)}$$

Potentials from excited states are marked with an asterisk and the oxidation state of the photosensitizer is n within these equations. The estimated excited-state potentials of the photocatalyst (E^*_{red} and E^*_{ox}) can be utilized to evaluate the thermodynamic feasibility for an excited-state quenching by any given substrate with known redox properties. Unsurprisingly, endergonic driving forces will result in diminished electron transfer rate constants or even to the absence of quenching. This also holds true for energy transfer, although excited-state equilibria between the energy donor and energy acceptor can result in repopulation of the excited state of the photosensitizer in case of small energy differences between these two counterparts.[100,125,136] These thermodynamic aspects are also discussed in more detail in the following paragraphs.

A combination between thermodynamic and kinetic parameters (i.e., the driving force and the rate constant for electron transfer) was introduced by Rudolph A. Marcus in 1956.[137] The details are beyond the scope of this perspective, but, from a qualitative perspective, in the famous Marcus theory, a parabola dependence of the Gibbs free energy of the electron transfer ΔG_{et} and the reorganization energy λ is presented (red parabola of the inset of Figure 8).[138–140] For reasonably small values of ΔG_{et}, the electron transfer rate increases with an increasing driving force (as highlighted in green in the inset of Figure 8). Notably, this analysis of Marcus also predicts a so-called inverted region with larger driving force but slower electron transfer rate constants (as highlighted in orange in the inset of Figure 8).[141] In practice, the large reorganization energies of the electron transfer process prevent in most cases this observation of the inverted region in intramolecular electron transfer[142] and the diffusion limit of the solvent (blue dotted line in Figure 8) limits the observable rate constant (represented in black in the inset of Figure 8) to k_{diff}.[139,143–146] In an empirical approach, Rehm and Weller reported an equation to analyze the dependence of electron transfer rate constant k_{et} on the Gibbs free energy (ΔG) for the photoinduced excited-state quenching step from an excited PS (PS*) to an electron donor or acceptor (Q) based on Equations 7 and 8.[135,147] The Gibbs free energy for the electron transfer step in this equation can be calculated as $\Delta G_{et} = E_{1/2}(Q) - E_{1/2}(PS^*)$.

$$k_{et} = \frac{k_{diff}}{1 + \frac{k_{-diff}}{Z}\left[\exp\left(\frac{\Delta G_{et}}{RT}\right) + \exp\left(\frac{\Delta G^{\#}_{et}}{RT}\right)\right]} \quad \text{(Equation 7)}$$

$$\Delta G^{\#}_{et} = \frac{\Delta G_{et}}{2} + \left(\left(\frac{\Delta G_{et}}{2}\right)^2 + \left(\frac{\lambda}{4}\right)^2\right)^{\frac{1}{2}} \quad \text{(Equation 8)}$$

$$\text{In acetonitrile}: k_{et} = \frac{2\,x10^{10}\,M^{-1}s^{-1}}{1 + 0.25\left[\exp\left(\frac{\Delta G_{et}}{RT}\right) + \exp\left(\frac{\Delta G^{\#}_{et}}{RT}\right)\right]} \quad \text{(Equation 9)}$$

In this equation, k_{diff} and k_{-diff} represent the diffusion rate constant and the dissociation rate constant of the encounter

Please cite this article in press as: De Kreijger et al., From photons to reactions: key concepts in photoredox catalysis, Chem Catalysis (2024), https://doi.org/10.1016/j.checat.2024.101110

CellPress

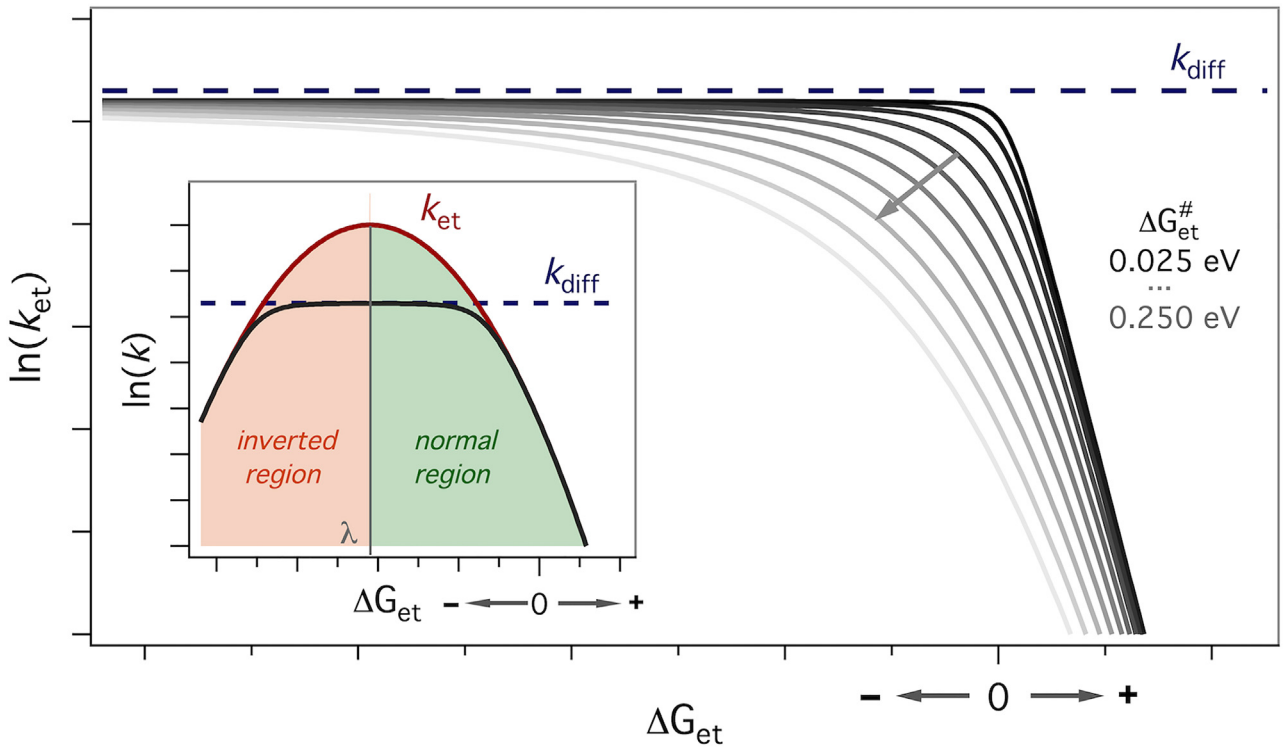

Figure 8. Evolution of the rate constants k_{et} of electron transfer as a function of driving force ΔG_{et} with different free energies of activation $\Delta G^{\#}_{et}$

This evolution was calculated using the empirical equation introduced by Weller and Rehm (Equation 7). The inset presents an illustration of electron transfer rate constants based on Marcus theory (k_{et}, red) and the observed rate constant (black).[139,148] The diffusional rate constant (k_{diff}) is presented as dotted blue line. For the parabola based on Marcus theory in the inset, the normal and inverted region are highlighted in green and orange, respectively.

complex (see Figure 1), respectively. The reorganization energy λ, as introduced by Marcus theory, is one parameter of the Gibbs free energy of activation ($\Delta G^{\#}_{et}$) for electron transfer. Weller and Rehm determined a pre-exponential Arrhenius factor of 0.25 $\left(=\frac{k_{-diff}}{Z}\right)$ in acetonitrile based on the collision factor Z and the diffusional encounter dissociation k_{-diff}.[147] With a diffusion limit of $2 \times 10^{10}\,M^{-1}s^{-1}$, the Weller Rehm equation in acetonitrile provides Equation 9. It is worth mentioning that the approach of Weller and Rehm only takes into consideration the diffusion limit at high driving forces within the respective solvent (k_{diff}), and a possible inverted region as presented by Marcus theory is thus not accounted for.

In practice, the magnitude of the Gibbs free energy of activation ($\Delta G^{\#}_{et}$, Equation 8) impacts the transition toward diffusion-limited processes. Indeed, smaller values of $\Delta G^{\#}_{et}$ result in a more abrupt change between the increasing electron transfer rate constants and the plateau close to the diffusional limit k_{diff} (Figure 8). A thermodynamic-like approach to describe $\Delta G^{\#}_{et}$ and the relation of Gibbs free energy and electron transfer rate constant has been proposed by Agmon and Levine.[149,150] Their approach has a qualitatively similar relation to the empirical equation of Rehm and Weller and is hence not discussed here in further detail. In general, spectroscopic measurements with a series of ED or EA molecules with known redox potentials can provide insights into the driving-force dependence of the excited-state quenching.[151] Recent reports utilized such analyses to provide very different insights into photophysical systems.[115] The group of Schanze analyzed the excited-state quenching of a short-lived and non-luminescent radical anion for the electron transfer with activated aryl halides to obtain a better understanding into the excited-state reactivity and estimate the excited-state oxidation potential of the radical anion.[152] For a luminescent acridinium catalyst developed by the Hansmann group with a two-electron reduction wave, the Rehm-Weller analysis allowed the determination of the excited-state potential and the one-electron reduction potential of the photocatalyst.[153] In a comparative study, Wenger and coworkers investigated a chromium complex with a spin-flip excited state and a ruthenium complex with a metal-to-ligand charge transfer excited state.[154] The determination of rate constants with different EDs enabled an analysis with the equation of Rehm and Weller and in combination with transient absorption spectroscopy revealed similar abilities for reductive excited-state quenching in both complexes despite their different excited-state characters.

Similar to the analysis of excited-state electron transfer quenching, an analysis of excited-state quenching by energy transfer is possible. Unsurprisingly, the energy difference between the energy donor (EnD) and the energy acceptor (EnA) has an influence on the energy transfer quenching rate constant

Please cite this article in press as: De Kreijger et al., From photons to reactions: key concepts in photoredox catalysis, Chem Catalysis (2024), https://doi.org/10.1016/j.checat.2024.101110

k_{EnT}. A comparably simple equation was introduced by Sandros considering a Boltzmann distribution for the energy transfer between donor and acceptor (Equation 10).[155]

$$k_{EnT} = \frac{k_{diff}}{1+\exp\left(\frac{\Delta G_{EnT}}{RT}\right)} \quad \text{(Equation 10)}$$

Following this equation, the energy transfer rate constant k_{EnT} is limited by the diffusion rate constant k_{diff} for large driving forces (ΔG_{EnT}, where $\Delta G_{EnT} = E_{EnA} - E_{EnD}$) and the observable rate constant is dependent on the temperature T. As this equation was sometimes unsuited to explain spectroscopic observations,[156,157] a so-called nonvertical energy transfer was later introduced, where Balzani and coworkers developed a more general equation to account for energy transfer with more distorted excited states (Equation 11).[157]

$$k_{EnT} = \frac{k_{diff}}{1+\exp\left(\frac{\Delta G_{EnT}}{RT}\right)+\frac{k_{-diff}}{Z}\exp\left(\frac{\Delta G^{\#}_{EnT}}{RT}\right)} \quad \text{(Equation 11)}$$

Equation 11 is very similar to Equation 10 introduced by Sandros, but it is extended with an additional term for the free energy of activation ($\Delta G^{\#}_{EnT}$) to account for an intrinsic barrier of the elementary step. This is especially important for distorted excited states with respect to the ground state, while for non-distorted (or weakly distorted) excited states, the third term of the denominator of Equation 11 is neglectable and the equation introduced by Sandros is again suitable to describe the correlation between driving force and energy transfer rate constant. Due to the fact that the same hypotheses and approximations as for excited-state quenching were used, a close similarity to the equation for electron transfer (Equation 7) is unsurprising and the intrinsic barrier introduced by the activation energy ($\Delta G^{\#}_{EnT}$) can be calculated based on the different relationships presented by Weller-Rehm (Equation 8), Marcus, or Agmon and Levine.[137,140,141,147,149]

In a recent report, a photophysical analysis with different sensitizers was performed to gain new insights on the sensitized *E* to *Z* isomerization of the double bond of alkenyl boron substrates.[158] Analysis with photosensitizers of different triplet energies and a thermal bond activation model (Equation 10) enabled experimental estimations of the triplet energies of both isomers and revealed an energy difference of 0.14 eV between the isomers. Subsequently, a spectroscopy-guided choice of a suitable photocatalyst was utilized to obtain enhanced product formation with shorter irradiation times and a metal-free sensitizer.

Overall, the determination of the excited-state quenching process is one of the key steps in photocatalysis to understand the interactions between the photocatalyst and the quencher. In addition to the differentiation between energy and electron transfer processes, careful considerations of thermodynamic aspects have to be realized for the design of efficient applications. However, even with a large driving force, knowledge of the elementary step, and a reasonable quenching, a successful subsequent reactivity is not guaranteed, as discussed in the next section.

CAGE ESCAPE FOLLOWING EXCITED-STATE ELECTRON TRANSFER

Immediately after electron transfer, the charge-separated state, i.e., the reduced/oxidized photosensitizer, and the oxidized/reduced quencher are still intimately enclosed within a solvent cage. In order for any photoredox catalytic reaction to be efficient, these species must undergo a process called cage escape; i.e., they must escape the solvent cage and create a new solvation layer around them. This process was first introduced in 1934 by Franck and Rabinowitsch[159,160] but was only experimentally verified several years later by Lyon and Levy, who performed crossover experiments using mixtures of azomethane and perdeuterated azomethane in the gas phase and in isooctane solutions.[161] As of today, there is no clear theory to describe the cage escape process and to predict the corresponding yields (Φ_{CE}). In addition, the factors that impact Φ_{CE} are not well defined and correlations have been established with parameters such as solvent polarity and viscosity,[162–166] the driving force for electron transfer,[167,168] the spin states,[163,164,169–172] as well as ionic strength effects.[165,166,169,173] It is, however, of paramount importance to first understand and subsequently ideally control these cage escape yields as they have been shown to ultimately impact the overall yields of photoredox catalysis reactions.[163,174,175] The factors that influence cage escape yields have also recently been reviewed and will thus only be discussed in the context of this tutorial review.[176]

Nowadays, these cage escape yields are straightforwardly measured by comparative actinometry techniques using Equations 12 and 13. In these equations, the relative concentration generated from the oxidized PS ($PS^{\bullet+}$) or reduced PS ($PS^{\bullet-}$) after excited-state electron transfer or from the oxidized or reduced (sacrificial) ED or EA are compared with the relative concentration of a reference actinometer (ES_{Ref}). Here, the procedure is exemplary developed for a reductive quenching process, but this can be treated for oxidative quenching processes in the same way. By transient absorption spectroscopy, the changes in absorbance of the actinometer ($\Delta A_{ES_{Ref}}$) upon excitation as well as the change in absorbance of the reduced PS after electron transfer (ΔA_{PS^-}) or of the oxidized donor is determined. Together with the changes of molar absorption coefficient of the actinometer ($\Delta\varepsilon_{ES_{Ref}}$) and the photoproduct after electron transfer ($\Delta\varepsilon_{PS}-$) at their respective detection wavelengths, the relative concentration of both species can be calculated ($\Delta[PS^{-}]$ and $\Delta[ES_{Ref}]$ in Equation 13). The change in molar absorption coefficient ($\Delta\varepsilon$) for the actinometer is known from the literature in some cases or can be determined by variable power excitation measurements using transient absorption measurements, whereas the $\Delta\varepsilon$ values of the oxidized or reduced photosensitizers can be determined by photolysis,[177] spectroelectrochemistry,[178] or using transient absorption spectroscopy with reference electron acceptors or electron donors.[179,180] It is important to determine the changes in molar absorption coefficient in the same solvent in which the reaction is performed as some species can experience large changes in molar absorption coefficient with solvent. To allow a meaningful comparison between relative concentrations of the actinometer and photoproducts after electron transfer, both solutions are normalized by

Please cite this article in press as: De Kreijger et al., From photons to reactions: key concepts in photoredox catalysis, Chem Catalysis (2024), https://doi.org/10.1016/j.checat.2024.101110

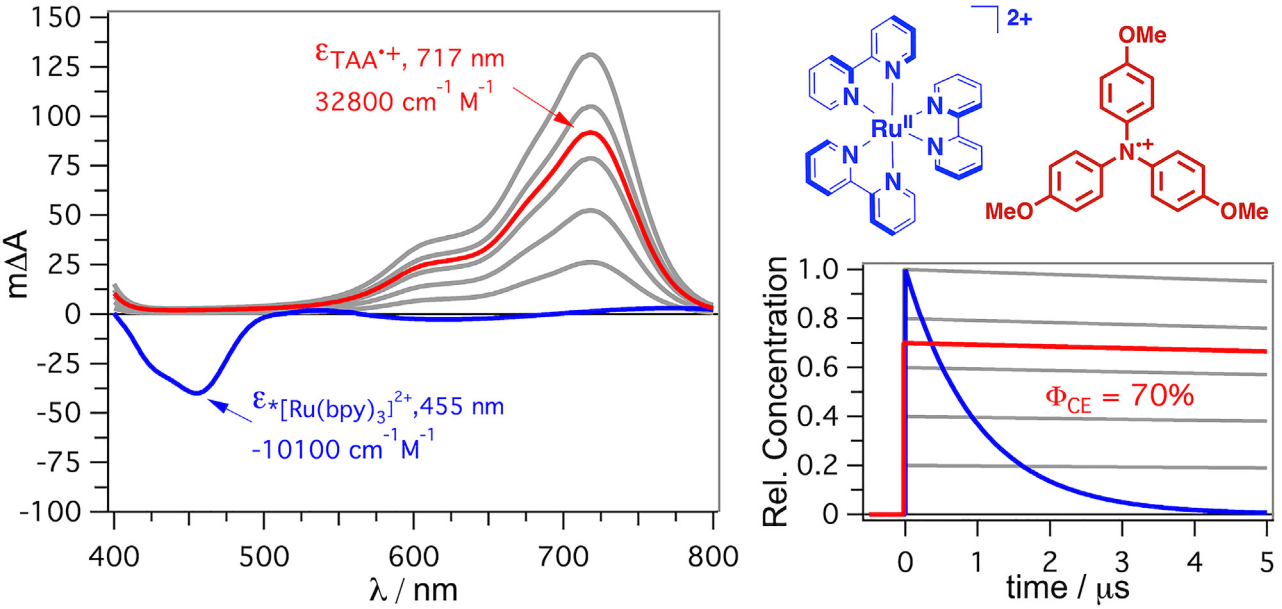

Figure 9. Method for determining cage escape yield

Left: simulated transient absorption spectra showing the changes in absorption corresponding to the absorption of oxidized tri-*p*-anisylamine ($TAA^{\bullet+}$) alongside the changes of absorption of the $[Ru(bpy)_3]^{2+}$ actinometer (blue). Right: relative concentration of $TTA^{\bullet+}$ based on the ΔAbs changes recorded at 717 nm and the bleach caused by the excited-state of $^{3*}[Ru(bpy)_3]^{2+}$ (blue) at 455 nm. The traces for the relative concentrations with a cage escape yield calculated based on the respective extinction coefficients[182–186] for the formation of $TAA^{\bullet+}$ between 0% and 100% are provided in gray and the simulated spectrum and kinetic trace for isoabsorptive solutions with 70% is highlighted in red. For simplicity, 100% quenching of the excited state (leading to $\Phi_{CE} = \Phi$) is assumed. Further details are explained in the text.

their relative absorptances at the excitation wavelength λ_{exc} to account for differences in the number of absorbed photons. These corrections by $1–10^{-AbsRef}$ and $1–10^{-AbsPS}$ are performed based on the respective ground-state absorbance (Abs) of both solutions at the excitation wavelength.

$$\Phi_{CE} = \frac{\Phi}{\%PL_{Quenched}} \times \text{with } \%PL_{Quenched} = \left(1 - \frac{PLI}{PLI_0}\right) = \left(1 - \frac{\tau}{\tau_0}\right) \quad \text{(Equation 12)}$$

$$\Phi = \left(\frac{\frac{\Delta A_{PS^-}}{\Delta \varepsilon_{PS^-}}}{\frac{\Delta A_{ES_{Ref}}}{\Delta \varepsilon_{ES_{Ref}}}}\right)\left(\frac{1 - 10^{-Abs_{Ref}(\lambda_{exc})}}{1 - 10^{-Abs_{PS}(\lambda_{exc})}}\right) = \left(\frac{\Delta[PS^-]}{\Delta[ES]_{Ref}}\right)\left(\frac{1 - 10^{-Abs_{Ref}(\lambda_{exc})}}{1 - 10^{-Abs_{PS}(\lambda_{exc})}}\right) \quad \text{(Equation 13)}$$

$$\Phi = \left(\frac{\frac{\Delta A_{PS^-}}{\Delta \varepsilon_{PS^-}}}{\frac{\Delta A_{ES_{Ref}}}{\Delta \varepsilon_{ES_{Ref}}}}\right) = \left(\frac{\Delta[PS^-]}{\Delta[ES]_{Ref}}\right) \text{ for isoabsorptive solutions} \quad \text{(Equation 14)}$$

Final Φ_{CE} values are obtained by comparing the relative yield of the reduced PS after electron transfer or of the oxidized donor produced (Φ) to the percentage of quenched photoluminescence ($\%PL_{Quenched}$). This percentage of quenched photoluminescence is determined via time-resolved or steady-state measurements in the absence (τ_0, PLI_0) and presence (τ, PLI) of quencher. A linear regression of all data points by constraining the y intercept at 0 provides a slope that corresponds to the cage escape yield value.[163,181] Figure 9 illustrates a possible spectroscopic measurement for the determination of relative concentrations of an oxidized triarylamine derivative with a large change in molar absorption coefficient ($\Delta\varepsilon = 32{,}800\ M^{-1}cm^{-1}$ in acetonitrile) and $[Ru(bpy)_3]^{2+}$ as actinometer ($\Delta\varepsilon = -10{,}100\ M^{-1}cm^{-1}$ in acetonitrile), assuming isoabsorptive solutions at the excitation wavelength and complete excited-state quenching for the reductive quenching process ($\%PL = 100\% = 1$).[182–186] Recently, a step-by-step protocol to determine the cage escape yield in solution using relative actinometry was published by our group, including hints, pitfalls, and more details about the individual steps.[187] Methods using isoabsorptive solutions of photosensitizer and actinometer allow to simplify Equation 13 into Equation 14. Alternative methods include determining Φ_{CE} at high concentration of quencher where almost all of the excited states are quenched. Although this approach is appropriate, there are some instances where cage escape yields decrease at high quencher concentration, either due to kinetic salt effects or due to the fact that the quencher becomes part of the cage.[188] While our idealized picture in Figure 9 indicates a direct determination of one of the photoproducts, spectral overlap between the transient absorption signals of the oxidized

Please cite this article in press as: De Kreijger et al., From photons to reactions: key concepts in photoredox catalysis, Chem Catalysis (2024), https://doi.org/10.1016/j.checat.2024.101110

and reduced species can lead to more complicated cases, where several molar absorption coefficients need to be considered to determine the actual concentration of the photoproducts.

Due to the fact that the cage escape yield Φ_{CE} is normalized by relative excited-state quenching (Equation 12), the absolute values between different photosensitizer, quencher, and different conditions can be directly compared. On the other hand, for a specific catalysis, the apparent relative yield (Φ) of the photoproducts under the actual reaction conditions might be different from the cage escape yield (Φ_{CE}). This is especially relevant for conditions that do not allow for efficient excited-state quenching. These diminished quenching efficiencies can, for example, result from comparably low concentrations of the quencher, interference with other undesired quenching processes within the solution, and/or (very) short excited-state lifetimes of the photosensitizer (see Figure 6 and Equation 4). As a consequence, even with a high cage escape yield after excited-state quenching, the relative formation of the desired photoproduct in solution after electron transfer can be small. Furthermore, within the progress of a reaction, concentration of different species in solution change and the relative efficiency of a certain pathway can change over time. These aspects highlight the complicated interplay between excited-state quenching, relative quenching efficiencies, in-cage charge recombination, cage escape, and the different rate constants of the individual processes.[189]

The impact of cage escape yields on overall photoredox catalysis reaction yields was very recently established using an iron(III) photosensitizer,[163,174] itself pioneered by Wärnmark and coworkers.[190] This photosensitizer was used to perform a dehalogenation reaction using green light irradiation. This reaction occurs via the excited-state reduction of the photosensitizer that can then transfer an electron to the organic substrate that undergoes dehalogenation. It can thus be hypothesized that the cage escape yield between the reduced photosensitizer and the oxidized ED can drastically impact the overall yield. As such, the cage escape yields with the iron photosensitizers and quenchers such as dimethylaniline, dimethyltoluidine, and tri-*p*-tolylamine were determined in different solvents. Very low cage escape yields (<0.1) were determined in acetonitrile and dimethylformamide, while these yields reached values greater than 0.36 in dichloromethane. These cage escape yields were thus shown to impact the overall reaction yield as the reaction proceeded efficiently (>90% conversion) only when dichloromethane was used. In solvents where the cage escape yields were small, the dehalogenation reaction yields dropped to values smaller than 30% after 24 h of irradiation. A related study comparing Ru(II), Ir(III), and Fe(III) photosensitizers also highlighted a change in reactivity depending on the photosensitizers and it seemed that cage escape yields likely played an important role.[174]

Very recently, Wenger and coworkers investigated the impact of cage escape yields on overall reaction yields using two photosensitizers, one based on Ru(II) and one based on Cr(III). The ruthenium-based photosensitizer exhibited triplet metal-to-ligand charge transfer excited state, while the chromium complex exhibited a spin-flip excited state. The cage escape yields were investigated in acetonitrile with a series of 12 EDs and were consistently significantly larger for the Ru(II) photosensitizer (Φ_{CE} between 0.35 and 0.87) than the Cr(III) one (Φ_{CE} between 0.07 and 0.19). The proposed hypothesis for this difference in cage escape yields was related to Marcus theory and the different driving forces for charge recombination within the geminate radical pair. The geminate charge recombination between the oxidized ED and the reduced photosensitizer within the solvent cage was more favored for the ruthenium photosensitizer than for the chromium catalyst. This fact results from the different redox potentials between the two sensitizers, which resulted in a geminate charge recombination with different driving forces for the two photosensitizers. For the ruthenium catalyst, the charge recombination driving force within the solvent cage was more favorable compared to the chromium catalyst. As a consequence, the rate constant for charge recombination is located further in the Marcus inverted region (see also Figure 8) and this process is comparably slow. In contrast, charge recombination was closer to the normal region for the chromium photosensitizer and geminate charge recombination was therefore dominant. As a consequence, the slower charge recombination of the geminate radical pair with ruthenium as photosensitizer—and subsequently a smaller rate constant for this process; see k_{GCR} in Figure 1—resulted in a higher relative contribution for the cage escape pathway within the decay pathways of this radical pair. To allow a comparison between both sensitizers, the same rate constant for cage escape k_{CE} was assumed for both complexes and, consequently, the differences in the geminate charge recombination rate constants k_{GCR} was used to rationalize the increased cage escape yields for smaller recombination rate constants. The authors further expanded their investigation in an attempt to correlate cage escape yields with reaction yields. To do so, they investigated three benchmark photocatalytic reactions: an aerobic hydroxylation, a reductive debromination, and an aza-Henry reaction. In all three cases, the rate of product formation proceeded more efficiently with the Ru(II) photosensitizer than with the Cr(III) photosensitizer and correlated well with the cage escape yields determined by transient absorption spectroscopy.

While an analysis based on Marcus theory could rationalize the observations of cage escape yields in the comparison between ruthenium and chromium photosensitizers, other parameters have also been shown to significantly impact these yields.[176] Recently, a study focusing of Ru(II), Os(II), Ir(III), and Fe(III) photosensitizers proposed that the spin state of the geminate radical pair was a key contributor to the cage escape yields after excited-state quenching via electron transfer.[191]

REACTION QUANTUM YIELD

Moving away from individual steps to full catalytic cycles, the determination of the overall efficiency of the photocatalysis becomes interesting. The photochemical quantum yield for a photoreaction Φ_{Rxn} correlates the amount of product formed with the number of photons absorbed by the photosensitizer (Equation 15).

$$\Phi_{Rxn} = \frac{n_{product}}{n_{absorbed\ photons}} \quad \text{(Equation 15)}$$

Please cite this article in press as: De Kreijger et al., From photons to reactions: key concepts in photoredox catalysis, Chem Catalysis (2024), https://doi.org/10.1016/j.checat.2024.101110

To analyze the reaction quantum yield, the determination of product formation over time is needed together with the number of photons absorbed after the respective irradiation time. Kinetic monitoring of a light-driven reaction can be performed in a variety of different reaction setups. Although the vessel and setup used for photochemical studies may vary, these studies require a calibrated light source to understand the relationship between absorbed photons and the reaction rates or the photochemical quantum yield. In principle, white light sources such as Xe arc lamps can be used, but narrow-band or monochromatic light simplifies the relationship between absorbed photons and the reaction yield. Modern high-output LEDs provide relatively cheap light sources, where a variety of different wavelengths can be selected. Intense continuous-wave lasers can also be used as a light source, although care must be taken to avoid excessive light flux, which might lead to higher-order absorptive processes.[192,193]

Light sources can be calibrated against radiometers such as thermopiles or piezoelectric radiometers, which themselves are calibrated to read absolute flux values. However, a common drawback of such instruments is their cost and the need to frequently recalibrate to compensate for any loss in sensitivity with use. As a result, chemical actinometers are often employed as an alternative.[194,195] Chemical actinometers are simple and well-studied photochemical systems that possess known reaction quantum yield (Φ_{Rxn}) values over a range of wavelengths. In addition, chemical actinometers are easily adapted to a variety of non-traditional reactor vessel types, including larger batch, photo-microfluidic,[196] and more traditional flow-through reactors.

Chemical actinometers should ideally have robust photochemical properties and typically be inexpensive or easily prepared. Additionally, these reactions should show no dark reactivity and have spectral features that enable facile monitoring of the reaction rate. In general, the chemical quantum yield is defined for a given actinometer at a specified wavelength under certain conditions. The ferrioxalate actinometer is a well-known standard, although its light sensitivity (QY > 1) can complicate the calibration process.[194] Numerous alternative actinometers, which cover a significant wavelength range, are known and interested readers are referred to the appropriate literature.[195]

Experimentally, in order to determine the intensity of a light source, a solution of the actinometer is illuminated and the reaction rate is quantified and converted to the light intensity using Equation 16:

$$-\frac{d[Act]}{dt} = I_0\phi\left(1 - 10^{-\varepsilon l[Act]}\right) \qquad \text{(Equation 16)}$$

In this equation, I_0 is the light intensity, ε the molar absorption coefficient, and l is the sample pathlength. In many cases, it is advantageous to prepare solutions such that the solution absorbance at the wavelength of interest is greater than two so that light absorbance can be assumed to be quantitative (less than 1% transmitted). Under these conditions, Equation 16 can be written as Equation 17, where k_0 (in $M^{-1}\ s^{-1}$) is the zeroth order rate constant. This assumption is particularly useful when using small, or irregularly shaped, reaction vessels such as NMR tubes.

$$I_0 = \frac{k_0}{\phi} \qquad \text{(Equation 17)}$$

Several techniques, such as UV-visible absorption or NMR spectroscopy, can be used to monitor the reaction of the actinometer. Once the light source is calibrated against the actinometer, the unknown reaction of interest can be monitored with a known photon flux incident per unit of time. The relationship between the observed reaction rate and the photon flux can then be related back to a quantum yield (Φ_{Rxn}, Equation 15).

NMR spectroscopy has become a common technique for monitoring photochemical reactions.[197–201] In contrast to many other techniques, the small size of common NMR tubes requires special attention due to their narrow cylindrical shape, which provides a limited and often ill-defined absorption pathlength. Although high concentrations can be used to achieve sufficient absorption to guarantee low light transmission, reactions performed in high concentrations can impact solvent viscosity, resulting in erroneous rate constants.[202] In order to balance these effects, Reibarkh and coworkers suggested performing multiple trials of a given actinometer over a series of increasing concentrations.[198,202] The group recently used this technique to monitor the progression of a photoinduced, iron-catalyzed cycloisomerization of an alkynol to cyclic enol ethers.[197] Monitoring the reaction progress via NMR measurements resulted in the detection of unstable intermediates that were not observed by other techniques, such as high-pressure liquid chromatography (HPLC). In addition to structural information normally afforded from NMR spectra, the authors were able to conclude that a paramagnetic Fe^{3+} species was not generated during the reaction due to the sharpness of all of the observed peaks. By using the previously described actinometry method,[8] the authors determined that 33% of incident photons lead to product formation.

In another example, Pichette and coworkers recently reported the use of NMR-based actinometry to determine the reaction quantum yield of a photolabile bis-alkoxysilane.[200] The authors found that incorporating this silyl linker into mesoporous organosilica particles imparted novel light instability. The reaction quantum yield for linker breakage was determined using Reibarkh's method and was found to be 0.30 ± 0.09.[202] This value compared favorable against the relatively few other light breakable silica systems and provides an important benchmark for comparing the rate of nanoparticle degradation to the reaction quantum yield of the photolabile linker.

CONCLUSIONS AND FUTURE OUTLOOKS

In this tutorial review, we have highlighted the significance of various key parameters in photoredox catalysis. The exploration of these parameters using advanced spectroscopic techniques offers a robust tool for investigating the behavior and reactivity of photocatalytic systems. Moreover, a deeper understanding of excited-state reactivity, cage escape, and reaction quantum yield will be pivotal for advancing the field of photoredox catalysis. This will not only enable the development of more efficient

Please cite this article in press as: De Kreijger et al., From photons to reactions: key concepts in photoredox catalysis, Chem Catalysis (2024), https://doi.org/10.1016/j.checat.2024.101110

and selective systems but also open the way for the design of novel strategies for organic synthesis and sustainable chemical processes. Thus, developing research in this direction holds great promise for addressing current challenges and unlocking new opportunities and methodologies in the field of photo-induced chemical transformations. Several areas of focus to continue advancing the field of light-induced transformations can thus be proposed.

Excited states' properties and reactivity

Controlling and understanding the excited-state properties such as the redox potential, excited-state lifetime, and excited-state energy play an important role in exerting fine control over reaction mechanisms of photocatalytic processes.[203] In the development of photosensitizers based on Earth-abundant metals for photocatalysis applications, leveraging short excited-state lifetimes represents a significant challenge. However, as detailed in this perspective, exploiting pre-association through non-covalent interactions or coordination bonding can facilitate efficient charge transfer and promote subsequent productive reaction pathways. Controlling the reactivity of a photosensitizer by tuning its coordination sphere presents an interesting avenue in the field of photocatalysis, akin to the recent work of Nocera and coworkers. Therefore, although the development of long-lived excited states based on Earth-abundant photosensitizers still represents an important research avenue, the development of strategies to pre-associate quencher with short-lived excited-state Earth-abundant photosensitizers will probably allow the field to efficiently move forward.

Control reaction conditions

Controlling the reaction conditions such as the reaction time, the light source and power, temperature, concentration, solvent and stoichiometry is of paramount importance in determining reactivity and products distribution for a given photocatalytic process. Thus, as emphasized by other researchers, the need for standardized protocol and irradiation setup is paramount.[204–206] The field of photoredox catalysis could also benefit from a clearer understanding of the impact of sacrificial electron donors or electron acceptors (SED/SEA) on the overall reaction. There are indeed reports where two distinct photosensitizers are used that generated different product distributions.[174,207] However, if the same mechanistic steps are initially involved, they should give the same product distribution unless alternative stabilization/destabilization of transition states are accessible with the different photosensitizers. Even more, a screening of sacrificial reagents is often carried out with the sole purpose of maximizing the yield of a product. However, in some case, different product distributions are observed with different SED/SEA using the same photosensitizers. Hence, gaining a deeper understanding of the impact of the choice of PS, SED, and SEA will definitely move the field forward.

Photostability

In most cases, degradation of the photosensitizers is not addressed individually, but trying to replicate examples from the literature has shown that the photosensitizer is often degraded over the course of the reaction.[208–210] This raises questions related to the actual reaction mechanism, or evolution of the mechanism during the course of the photoredox catalysis, as intermediate PS degradation products or metal nanoparticles/metal oxides (in the case of transition metal PS) could potentially trigger mechanistic changes or contribute to the reaction yield.[208,211] This analysis is often performed for electrocatalytic reactions[212] and could thus help improve the reliability of some photoredox transformations. As the catalyst stability is highly dependent on the reaction environment, it can change over time, and careful analyses are needed to understand this aspect of catalysis. In that regard, we believe that it is important to develop novel, more robust photosensitizers and to investigate the recyclability. In a recent study, we have shown that polynuclear Ru(II) PS are much more photostable than $[Ru(bpy)_3]^{2+}$, with no signs of degradation over prolonged illumination. The iron complexes recently reported by Wärnmark and coworkers also show great photostability, both in solution[190] as well as in photocatalytic conditions,[163] where they have been recovered post reaction with yields greater than 88%.

Cage escape yields

As mentioned in the previous sections, cage escape yields play an important role in the observation of photo-products and in the overall chemical transformation. Parameters that influence cage escape yields are not well defined, but strategies exist to maximize those yields.[176,191] It is foreseen that maximizing the amount of charge-separated species could speed the corresponding reaction and, in some case, maybe even control product distribution. Hence, understanding factors that govern cage escape yields will be very important to continue moving the field of photoredox catalysis forward.

It is complicated to estimate the minimum cage escape yields that would be needed for an efficient photoreaction as the overall reaction yield also depends on the photon flux, the quenching rate constant, the electron transfer rate constant, and the rate constant associated with bond forming and bond breaking to generate the desired product. However, taking the examples presented into consideration as well as those recently reviewed,[176] we postulate that, with an efficient quenching rate constant and using commercially available LED irradiation setup, cage escape yields of at least 0.2–0.3 are needed for efficient photoredox catalytic transformations to occur in less than 16 h. Lower cage escape yields would result in inefficient/incomplete reaction or prolonged irradiation times.

ACKNOWLEDGMENTS

F.G. is a Chargé de Recherches of the Fonds de la Recherche Scientifique (FNRS). L.T.-G. is a Chercheur Qualifié of the Fonds de la Recherche Scientifique – FNRS. All the authors gratefully acknowledge the UCLouvain for financial support. L.T.-G. acknowledges the continuous support from the Fonds de la Recherche Scientifique (F.R.S.-FNRS, grant no. 40020332) as well as the Walloon Region (FRFS-WEL-T strategic axis) and the Action de Recherche Concertée through the project UNCAGED under grant no. 23/28-135.

AUTHOR CONTRIBUTIONS

S.D.K., F.G., and L.T.-G. wrote, edited, and revised the manuscript and created original figures.

DECLARATION OF INTERESTS

The authors declare no competing interests.

REFERENCES

1. Woodward, R.B., and Hoffmann, R. (1965). Stereochemistry of Electrocyclic Reactions. J. Am. Chem. Soc. *87*, 395–397. https://doi.org/10.1021/ja01080a054.
2. Woodward, R.B., and Hoffmann, R. (1965). Selection Rules for Sigmatropic Reactions. J. Am. Chem. Soc. *87*, 2511–2513. https://doi.org/10.1021/ja01089a050.
3. Woodward, R.B., Cava, M.P., Ollis, W.D., Hunger, A., Daeniker, H.U., and Schenker, K. (1963). The total synthesis of strychnine. Tetrahedron *19*, 247–288. https://doi.org/10.1016/S0040-4020(01)98529-1.
4. Tao, B., Schlingloff, G., and Sharpless, K. (1998). Reversal of regioselection in the asymmetric aminohydroxylation of cinnamates. Tetrahedron Lett. *39*, 2507–2510. https://doi.org/10.1016/S0040-4039(98)00350-5.
5. Millward, S.W., Henning, R.K., Kwong, G.A., Pitram, S., Agnew, H.D., Deyle, K.M., Nag, A., Hein, J., Lee, S.S., Lim, J., et al. (2011). Iterative in Situ Click Chemistry Assembles a Branched Capture Agent and Allosteric Inhibitor for Akt1. J. Am. Chem. Soc. *133*, 18280–18288. https://doi.org/10.1021/ja2064389.
6. Li, G., Chang, H.-T., and Sharpless, K.B. (1996). Catalytic Asymmetric Aminohydroxylation (AA) of Olefins. Angew. Chem. Int. Ed. *35*, 451–454. https://doi.org/10.1002/anie.199604511.
7. Hoffmann, R., and Woodward, R.B. (1965). Selection Rules for Concerted Cycloaddition Reactions. J. Am. Chem. Soc. *87*, 2046–2048. https://doi.org/10.1021/ja01087a034.
8. Corey, E.J., Yu, C.M., and Kim, S.S. (1989). A practical and efficient method for enantioselective allylation of aldehydes. J. Am. Chem. Soc. *111*, 5495–5496. https://doi.org/10.1021/ja00196a082.
9. Corey, E.J., and Link, J.O. (1989). A new chiral catalyst for the enantioselective synthesis of secondary alcohols and deuterated primary alcohols by carbonyl reduction. Tetrahedron Lett. *30*, 6275–6278. https://doi.org/10.1016/S0040-4039(01)93871-7.
10. Corey, E.J., and Gavai, A.V. (1988). Enantioselective route to a key intermediate in the total synthesis of ginkgolide B. Tetrahedron Lett. *29*, 3201–3204. https://doi.org/10.1016/0040-4039(88)85121-9.
11. Copéret, C., Adolfsson, H., Chiang, J.P., Yudin, A.K., and Sharpless, K.B. (1998). A simple and efficient method for the preparation of pyridine-N-oxides II. Tetrahedron Lett. *39*, 761–764. https://doi.org/10.1016/S0040-4039(97)10619-0.
12. Berend, S., Vrdoljak, A.L., Radic, B., Kalisiak, J., Radic, Z., Taylor, P., Fokin, V.V., and Sharpless, K.B. (2010). Characterizing the therapeutic efficacy of novel oximes synthesized by click chemistry against organophosphorous compounds poisoning. Toxicol. Lett. *196*, S254. https://doi.org/10.1016/j.toxlet.2010.03.849.
13. Adolfsson, H., Converso, A., and Sharpless, K. (1999). Comparison of amine additives most effective in the new methyltrioxorhenium-catalyzed epoxidation process. Tetrahedron Lett. *40*, 3991–3994. https://doi.org/10.1016/S0040-4039(99)00661-9.
14. Kim, J.H., and Scialli, A.R. (2011). Thalidomide: The Tragedy of Birth Defects and the Effective Treatment of Disease. Toxicol. Sci. *122*, 1–6. https://doi.org/10.1093/toxsci/kfr088.
15. Rehman, W., Arfons, L.M., and Lazarus, H.M. (2011). The rise, fall and subsequent triumph of thalidomide: lessons learned in drug development. Ther. Adv. Hematol. *2*, 291–308. https://doi.org/10.1177/2040620711413165.
16. Anastas, P.T., and Warner, J.C. (2000). Green Chemistry: Theory and Practice (Oxford University Press)). https://doi.org/10.1093/oso/9780198506980.001.0001.
17. Ciamician, G., and Silber, P. (1908). Chemische Lichtwirkungen. Ber. Dtsch. Chem. Ges. *41*, 1071–1080. https://doi.org/10.1002/cber.190804101211.
18. Hedstrand, D.M., Kruizinga, W.H., and Kellogg, R.M. (1978). Light induced and dye accelerated reductions of phenacyl onium salts by 1,4-dihydropyridines. Tetrahedron Lett. *19*, 1255–1258. https://doi.org/10.1016/S0040-4039(01)94515-0.
19. Van Bergen, T.J., Hedstrand, D.M., Kruizinga, W.H., and Kellogg, R.M. (1979). Chemistry of dihydropyridines. 9. Hydride transfer from 1,4-dihydropyridines to sp3-hybridized carbon in sulfonium salts and activated halides. Studies with NAD(P)H models. J. Org. Chem. *44*, 4953–4962. https://doi.org/10.1021/jo00394a044.
20. Studer, A., and Curran, D.P. (2014). The electron is a catalyst. Nat. Chem. *6*, 765–773. https://doi.org/10.1038/nchem.2031.
21. Vasudevan, A., Villamil, C., Trumbull, J., Olson, J., Sutherland, D., Pan, J., and Djuric, S. (2010). LOPHTOR: a convenient flow-based photochemical reactor. Tetrahedron Lett. *51*, 4007–4009. https://doi.org/10.1016/j.tetlet.2010.05.119.
22. Anderson, B.G., Bauta, W.E., and Cantrell, W.R., Jr. (2012). Development of an Improved Process for Doxercalciferol via a Continuous Photochemical Reaction. Org. Process Res. Dev. *16*, 967–975. https://doi.org/10.1021/op200346g.
23. Cantillo, D., Mateos, C., Rincon, J.A., de Frutos, O., and Kappe, C.O. (2015). Light-Induced C-H Arylation of (Hetero)arenes by In Situ Generated Diazo Anhydrides. Chem. Eur J. *21*, 12894–12898. https://doi.org/10.1002/chem.201502357.
24. Cantillo, D., de Frutos, O., Rincón, J.A., Mateos, C., and Kappe, C.O. (2014). Continuous Flow α-Trifluoromethylation of Ketones by Metal-Free Visible Light Photoredox Catalysis. Org. Lett. *16*, 896–899. https://doi.org/10.1021/ol403650y.
25. Cantillo, D., de Frutos, O., Rincon, J.A., Mateos, C., and Kappe, C.O. (2014). A Scalable Procedure for Light-Induced Benzylic Brominations in Continuous Flow. J. Org. Chem. *79*, 223–229. https://doi.org/10.1021/jo402409k.
26. Cantillo, D., de Frutos, O., Rincón, J.A., Mateos, C., and Kappe, C.O. (2014). A Continuous-Flow Protocol for Light-Induced Benzylic Fluorinations. J. Org. Chem. *79*, 8486–8490. https://doi.org/10.1021/jo5016757.
27. Nardello-Rataj, V., Alsters, P.L., and Aubry, J.-M. (2016). Industrial Prospects for the Chemical and Photochemical Singlet Oxygenation of Organic Compounds. In Liquid Phase Aerobic Oxidation Catalysis: Industrial Applications and Academic Perspectives, pp. 369–395. https://doi.org/10.1002/9783527690121.ch22.
28. Basso, A., and Capurro, P. (2020). 3 Recent applications of photochemistry on large-scale synthesis (2015–2019). In Photochemistry, *Volume 48*, S. Protti and C. Raviola, eds. (The Royal Society of Chemistry), pp. 293–321. https://doi.org/10.1039/9781839162114-00293.
29. Turconi, J., Griolet, F., Guevel, R., Oddon, G., Villa, R., Geatti, A., Hvala, M., Rossen, K., Göller, R., and Burgard, A. (2014). Semisynthetic Artemisinin, the Chemical Path to Industrial Production. Org. Process Res. Dev. *18*, 417–422. https://doi.org/10.1021/op4003196.
30. Lakowicz, J.R. (2006). Principles of Fluorescence Spectroscopy, Third edition Edition (Springer).
31. Coppola, G.A., Pillitteri, S., Van der Eycken, E.V., You, S.-L., and Sharma, U.K. (2022). Multicomponent reactions and photo/electrochemistry join forces: atom economy meets energy efficiency. Chem. Soc. Rev. *51*, 2313–2382. https://doi.org/10.1039/D1CS00510C.
32. Capaldo, L., and Ravelli, D. (2020). The Dark Side of Photocatalysis: One Thousand Ways to Close the Cycle. Eur. J. Org. Chem. *2020*, 2783–2806. https://doi.org/10.1002/ejoc.202000144.
33. Murov, S.L., Carmichael, I., and Hug, G.L. (1993). Handbook of Photochemistry, 2nd edition (New York: Marcel Dekker, Inc.).

34. Sutin, N. (1982). Nuclear, electronic, and frequency factors in electron transfer reactions. Acc. Chem. Res. *15*, 275–282. https://doi.org/10.1021/ar00081a002.

35. Deetz, A.M., Troian-Gautier, L., Wehlin, S.A.M., Piechota, E.J., and Meyer, G.J. (2021). On the Determination of Halogen Atom Reduction Potentials with Photoredox Catalysts. J. Phys. Chem. A *125*, 9355–9367. https://doi.org/10.1021/acs.jpca.1c06772.

36. Vauthey, E. (2022). Elucidating the Mechanism of Bimolecular Photoinduced Electron Transfer Reactions. J. Phys. Chem. B *126*, 778–788. https://doi.org/10.1021/acs.jpcb.1c10050.

37. Chiorboli, C., Indelli, M.T., Rampi Scandola, M.A., and Scandola, F. (1988). Salt effects on nearly diffusion controlled electron-transfer reactions: bimolecular rate constants and cage escape yields in oxidative quenching of tris(2,2'-bipyridine)ruthenium(II). J. Phys. Chem. *92*, 156–163. https://doi.org/10.1021/j100312a034.

38. Debye, P. (1942). Reaction Rates in Ionic Solutions. T. Electrochem. Soc. *82*, 265. https://doi.org/10.1149/1.3071413.

39. Buzzetti, L., Crisenza, G.E.M., and Melchiorre, P. (2019). Mechanistic Studies in Photocatalysis. Angew. Chem. Int. Ed. *58*, 3730–3747. https://doi.org/10.1002/anie.201809984.

40. Jin, Y., Zhang, Q., Wang, L., Wang, X., Meng, C., and Duan, C. (2021). Convenient C(sp3)–H bond functionalisation of light alkanes and other compounds by iron photocatalysis. Green Chem. *23*, 6984–6989. https://doi.org/10.1039/D1GC01563J.

41. Nielsen, M.K., Shields, B.J., Liu, J., Williams, M.J., Zacuto, M.J., and Doyle, A.G. (2017). Mild, Redox-Neutral Formylation of Aryl Chlorides through the Photocatalytic Generation of Chlorine Radicals. Angew. Chem. Int. Ed. *56*, 7191–7194. https://doi.org/10.1002/anie.201702079.

42. Gillespie, J.E., Fanourakis, A., and Phipps, R.J. (2022). Strategies That Utilize Ion Pairing Interactions to Exert Selectivity Control in the Functionalization of C–H Bonds. J. Am. Chem. Soc. *144*, 18195–18211. https://doi.org/10.1021/jacs.2c08752.

43. Gu, Z.-G., Liu, W., Yang, Q.-F., Zhou, X.-H., Zuo, J.-L., and You, X.-Z. (2007). Cyano-Bridged FeIII2CuII3 and FeIII4NiII4 Complexes: Syntheses, Structures, and Magnetic Properties. Inorg. Chem. *46*, 3236–3244. https://doi.org/10.1021/ic062267q.

44. Alonso, R., and Bach, T. (2014). A Chiral Thioxanthone as an Organocatalyst for Enantioselective [2+2] Photocycloaddition Reactions Induced by Visible Light. Angew. Chem. Int. Ed. *53*, 4368–4371. https://doi.org/10.1002/anie.201310997.

45. Wu, S., Žurauskas, J., Domański, M., Hitzfeld, P.S., Butera, V., Scott, D.J., Rehbein, J., Kumar, A., Thyrhaug, E., Hauer, J., and Barham, J.P. (2021). Hole-mediated photoredox catalysis: tris(p-substituted)biarylaminium radical cations as tunable, precomplexing and potent photooxidants. Org. Chem. Front. *8*, 1132–1142. https://doi.org/10.1039/D0QO01609H.

46. Juliá, F. (2022). Ligand-to-Metal Charge Transfer (LMCT) Photochemistry at 3d-Metal Complexes: An Emerging Tool for Sustainable Organic Synthesis. ChemCatChem *14*, e202200916. https://doi.org/10.1002/cctc.202200916.

47. May, A.M., and Dempsey, J.L. (2024). A new era of LMCT: leveraging ligand-to-metal charge transfer excited states for photochemical reactions. Chem. Sci. *15*, 6661–6678. https://doi.org/10.1039/D3SC05268K.

48. Gonzalez, M.I., Gygi, D., Qin, Y., Zhu, Q., Johnson, E.J., Chen, Y.-S., and Nocera, D.G. (2022). Taming the Chlorine Radical: Enforcing Steric Control over Chlorine-Radical-Mediated C–H Activation. J. Am. Chem. Soc. *144*, 1464–1472. https://doi.org/10.1021/jacs.1c13333.

49. Glaser, F., Aydogan, A., Elias, B., and Troian-Gautier, L. (2024). The great strides of iron photosensitizers for contemporary organic photoredox catalysis: On our way to the holy grail? Coord. Chem. Rev. *500*, 215522. https://doi.org/10.1016/j.ccr.2023.215522.

50. Hwang, S.J., Anderson, B.L., Powers, D.C., Maher, A.G., Hadt, R.G., and Nocera, D.G. (2015). Halogen Photoelimination from Monomeric Nickel(III) Complexes Enabled by the Secondary Coordination Sphere. Organometallics *34*, 4766–4774. https://doi.org/10.1021/acs.organomet.5b00568.

51. Hwang, S.J., Powers, D.C., Maher, A.G., Anderson, B.L., Hadt, R.G., Zheng, S.-L., Chen, Y.-S., and Nocera, D.G. (2015). Trap-Free Halogen Photoelimination from Mononuclear Ni(III) Complexes. J. Am. Chem. Soc. *137*, 6472–6475. https://doi.org/10.1021/jacs.5b03192.

52. Gygi, D., Gonzalez, M.I., Hwang, S.J., Xia, K.T., Qin, Y., Johnson, E.J., Gygi, F., Chen, Y.-S., and Nocera, D.G. (2021). Capturing the Complete Reaction Profile of a C–H Bond Activation. J. Am. Chem. Soc. *143*, 6060–6064. https://doi.org/10.1021/jacs.1c02630.

53. Kang, Y.C., Treacy, S.M., and Rovis, T. (2021). Iron-Catalyzed Photoinduced LMCT: A 1° C–H Abstraction Enables Skeletal Rearrangements and C(sp3)–H Alkylation. ACS Catal. *11*, 7442–7449. https://doi.org/10.1021/acscatal.1c02285.

54. Du, J., Yang, X., Wang, X., An, Q., He, X., Pan, H., and Zuo, Z. (2021). Photocatalytic Aerobic Oxidative Ring Expansion of Cyclic Ketones to Macrolactones by Cerium and Cyanoanthracene Catalysis. Angew. Chem. Int. Ed. *60*, 5370–5376. https://doi.org/10.1002/anie.202012720.

55. Rovis, T., Kang, Y.C., and Treacy, S.M. (2021). Iron-Catalyzed C(sp3)–H Alkylation through Ligand-to-Metal Charge Transfer. Synlett *32*, 1767–1771. https://doi.org/10.1055/s-0040-1720388.

56. Lian, P., Long, W., Li, J., Zheng, Y., and Wan, X. (2020). Visible-Light-Induced Vicinal Dichlorination of Alkenes through LMCT Excitation of CuCl2. Angew. Chem. Int. Ed. *59*, 23603–23608. https://doi.org/10.1002/anie.202010801.

57. Treacy, S.M., and Rovis, T. (2021). Copper Catalyzed C(sp3)–H Bond Alkylation via Photoinduced Ligand-to-Metal Charge Transfer. J. Am. Chem. Soc. *143*, 2729–2735. https://doi.org/10.1021/jacs.1c00687.

58. Xu, P., López-Rojas, P., and Ritter, T. (2021). Radical Decarboxylative Carbometalation of Benzoic Acids: A Solution to Aromatic Decarboxylative Fluorination. J. Am. Chem. Soc. *143*, 5349–5354. https://doi.org/10.1021/jacs.1c02490.

59. Chen, T.Q., Pedersen, P.S., Dow, N.W., Fayad, R., Hauke, C.E., Rosko, M.C., Danilov, E.O., Blakemore, D.C., Dechert-Schmitt, A.-M., Knauber, T., et al. (2022). A Unified Approach to Decarboxylative Halogenation of (Hetero)aryl Carboxylic Acids. J. Am. Chem. Soc. *144*, 8296–8305. https://doi.org/10.1021/jacs.2c02392.

60. Reichle, A., Sterzel, H., Kreitmeier, P., Fayad, R., Castellano, F.N., Rehbein, J., and Reiser, O. (2022). Copper(ii)-photocatalyzed decarboxylative oxygenation of carboxylic acids. Chem. Commun. *58*, 4456–4459. https://doi.org/10.1039/D2CC00570K.

61. Na, H., Watson, M.B., Tang, F., Rath, N.P., and Mirica, L.M. (2021). Photoreductive chlorine elimination from a Ni(iii)Cl2 complex supported by a tetradentate pyridinophane ligand. Chem. Commun. *57*, 7264–7267. https://doi.org/10.1039/D1CC02114A.

62. Shields, B.J., and Doyle, A.G. (2016). Direct C(sp3)–H Cross Coupling Enabled by Catalytic Generation of Chlorine Radicals. J. Am. Chem. Soc. *138*, 12719–12722. https://doi.org/10.1021/jacs.6b08397.

63. Weiss, M.E., Kreis, L.M., Lauber, A., and Carreira, E.M. (2011). Cobalt-Catalyzed Coupling of Alkyl Iodides with Alkenes: Deprotonation of Hydridocobalt Enables Turnover. Angew. Chem. Int. Ed. *50*, 11125–11128. https://doi.org/10.1002/anie.201105235.

64. Prina Cerai, G., and Morandi, B. (2016). Atom-economical cobalt-catalysed regioselective coupling of epoxides and aziridines with alkenes. Chem. Commun. *52*, 9769–9772. https://doi.org/10.1039/C6CC04410G.

65. Ociepa, M., Baka, O., Narodowiec, J., and Gryko, D. (2017). Light-Driven Vitamin B12-Catalysed Generation of Acyl Radicals from 2-S-Pyridyl Thioesters. Adv. Synth. Catal. *359*, 3560–3565. https://doi.org/10.1002/adsc.201700913.

66. Zhang, Z., Hilche, T., Slak, D., Rietdijk, N.R., Oloyede, U.N., Flowers, R.A., 2nd, and Gansäuer, A. (2020). Titanocenes as Photoredox

Catalysts Using Green-Light Irradiation. Angew. Chem. Int. Ed. *59*, 9355–9359. https://doi.org/10.1002/anie.202001508.

67. Sumiyama, K., Toriumi, N., and Iwasawa, N. (2021). Use of Isopropyl Alcohol as a Reductant for Catalytic Dehydoxylative Dimerization of Benzylic Alcohols Utilizing Ti−O Bond Photohomolysis. Eur. J. Org. Chem. *2021*, 2474–2478. https://doi.org/10.1002/ejoc.202100286.
68. Yamane, M., Kanzaki, Y., Mitsunuma, H., and Kanai, M. (2022). Titanium(IV) Chloride-Catalyzed Photoalkylation via C(sp3)–H Bond Activation of Alkanes. Org. Lett. *24*, 1486–1490. https://doi.org/10.1021/acs.orglett.2c00138.
69. Panetti, G.B., Yang, Q., Gau, M.R., Carroll, P.J., Walsh, P.J., and Schelter, E.J. (2022). Discovery and mechanistic investigation of photoinduced sp3 C–H activation of hydrocarbons by the simple anion hexachlorotitanate. Chem Catal. *2*, 853–866. https://doi.org/10.1016/j.checat.2022.02.013.
70. Tasnim, T., Ayodele, M.J., and Pitre, S.P. (2022). Recent Advances in Employing Catalytic Donors and Acceptors in Electron Donor–Acceptor Complex Photochemistry. J. Org. Chem. *87*, 10555–10563. https://doi.org/10.1021/acs.joc.2c01013.
71. Rathore, R., and Kochi, J.K. (2000). Donor/acceptor organizations and the electron-transfer paradigm for organic reactivity. In Advances in Physical Organic Chemistry (Academic Press), pp. 193–318. https://doi.org/10.1016/S0065-3160(00)35014-6.
72. Cantacuzène, D., Wakselman, C., and Dorme, R. (1977). Condensation of perfluoroalkyl iodides with unsaturated nitrogen compounds. J. Chem. Soc. Perk. T, 1365–1371. https://doi.org/10.1039/P19770001365.
73. Russell, G.A., and Wang, K. (1991). Electron transfer processes. 53. Homolytic alkylation of enamines by electrophilic radicals. J. Org. Chem. *56*, 3475–3479. https://doi.org/10.1021/jo00011a007.
74. Bunnett, J.F. (1978). Aromatic substitution by the SRN1 mechanism. Acc. Chem. Res. *11*, 413–420. https://doi.org/10.1021/ar50131a003.
75. Kandukuri, S.R., Bahamonde, A., Chatterjee, I., Jurberg, I.D., Escudero-Adán, E.C., and Melchiorre, P. (2015). X-Ray Characterization of an Electron Donor–Acceptor Complex that Drives the Photochemical Alkylation of Indoles. Angew. Chem. Int. Ed. *54*, 1485–1489. https://doi.org/10.1002/anie.201409529.
76. Zhang, H.-H., and Yu, S. (2019). Visible-Light-Induced Radical Acylation of Imines with α-Ketoacids Enabled by Electron-Donor–Acceptor Complexes. Org. Lett. *21*, 3711–3715. https://doi.org/10.1021/acs.orglett.9b01169.
77. Xie, S., Li, D., Huang, H., Zhang, F., and Chen, Y. (2019). Intermolecular Radical Addition to Ketoacids Enabled by Boron Activation. J. Am. Chem. Soc. *141*, 16237–16242. https://doi.org/10.1021/jacs.9b09099.
78. Sun, X., Wang, W., Li, Y., Ma, J., and Yu, S. (2016). Halogen-Bond-Promoted Double Radical Isocyanide Insertion under Visible-Light Irradiation: Synthesis of 2-Fluoroalkylated Quinoxalines. Org. Lett. *18*, 4638–4641. https://doi.org/10.1021/acs.orglett.6b02271.
79. Davies, J., Booth, S.G., Essafi, S., Dryfe, R.A.W., and Leonori, D. (2015). Visible-Light-Mediated Generation of Nitrogen-Centered Radicals: Metal-Free Hydroimination and Iminohydroxylation Cyclization Reactions. Angew. Chem. Int. Ed. *54*, 14017–14021. https://doi.org/10.1002/anie.201507641.
80. Li, J., Zhang, P., Jiang, M., Yang, H., Zhao, Y., and Fu, H. (2017). Visible Light as a Sole Requirement for Intramolecular C(sp3)–H Imination. Org. Lett. *19*, 1994–1997. https://doi.org/10.1021/acs.orglett.7b00533.
81. Li, Y., Mao, R., and Wu, J. (2017). N-Radical Initiated Aminosulfonylation of Unactivated C(sp3)–H Bond through Insertion of Sulfur Dioxide. Org. Lett. *19*, 4472–4475. https://doi.org/10.1021/acs.orglett.7b02010.
82. Sun, J., He, Y., An, X.-D., Zhang, X., Yu, L., and Yu, S. (2018). Visible-light-induced iminyl radical formation via electron-donor–acceptor complexes: a photocatalyst-free approach to phenanthridines and quinolines. Org. Chem. Front. *5*, 977–981. https://doi.org/10.1039/C7QO00992E.
83. Woźniak, Ł., Murphy, J.J., and Melchiorre, P. (2015). Photo-organocatalytic Enantioselective Perfluoroalkylation of β-Ketoesters. J. Am. Chem. Soc. *137*, 5678–5681. https://doi.org/10.1021/jacs.5b03243.
84. Morack, T., Mück-Lichtenfeld, C., and Gilmour, R. (2019). Bioinspired Radical Stetter Reaction: Radical Umpolung Enabled by Ion-Pair Photocatalysis. Angew. Chem. Int. Ed. *58*, 1208–1212. https://doi.org/10.1002/anie.201809601.
85. Cao, Z.-Y., Ghosh, T., and Melchiorre, P. (2018). Enantioselective radical conjugate additions driven by a photoactive intramolecular iminium-ion-based EDA complex. Nat. Commun. *9*, 3274. https://doi.org/10.1038/s41467-018-05375-2.
86. Fu, M.-C., Shang, R., Zhao, B., Wang, B., and Fu, Y. (2019). Photocatalytic decarboxylative alkylations mediated by triphenylphosphine and sodium iodide. Science *363*, 1429–1434. https://doi.org/10.1126/science.aav3200.
87. Bosque, I., and Bach, T. (2019). 3-Acetoxyquinuclidine as Catalyst in Electron Donor–Acceptor Complex-Mediated Reactions Triggered by Visible Light. ACS Catal. *9*, 9103–9109. https://doi.org/10.1021/acscatal.9b01039.
88. Liu, Q., Lu, Y., Sheng, H., Zhang, C.-S., Su, X.-D., Wang, Z.-X., and Chen, X.-Y. (2021). Visible-Light-Induced Selective Photolysis of Phosphonium Iodide Salts for Monofluoromethylations. Angew. Chem. Int. Ed. *60*, 25477–25484. https://doi.org/10.1002/anie.202111006.
89. Shibutani, S., Kodo, T., Takeda, M., Nagao, K., Tokunaga, N., Sasaki, Y., and Ohmiya, H. (2020). Organophotoredox-Catalyzed Decarboxylative C(sp3)–O Bond Formation. J. Am. Chem. Soc. *142*, 1211–1216. https://doi.org/10.1021/jacs.9b12335.
90. Tasnim, T., Ryan, C., Christensen, M.L., Fennell, C.J., and Pitre, S.P. (2022). Radical Perfluoroalkylation Enabled by a Catalytically Generated Halogen Bonding Complex and Visible Light Irradiation. Org. Lett. *24*, 446–450. https://doi.org/10.1021/acs.orglett.1c04139.
91. Lu, H., Wang, D.-y., and Zhang, A. (2020). Visible Light-Promoted Phosphine-Catalyzed Difluoroalkylation of Arenes and Heterocycles. J. Org. Chem. *85*, 942–951. https://doi.org/10.1021/acs.joc.9b02882.
92. Emmanuel, M.A., Greenberg, N.R., Oblinsky, D.G., and Hyster, T.K. (2016). Accessing non-natural reactivity by irradiating nicotinamide-dependent enzymes with light. Nature *540*, 414–417. https://doi.org/10.1038/nature20569.
93. Quint, V., Morlet-Savary, F., Lohier, J.-F., Lalevée, J., Gaumont, A.-C., and Lakhdar, S. (2016). Metal-Free, Visible Light-Photocatalyzed Synthesis of Benzo[b]phosphole Oxides: Synthetic and Mechanistic Investigations. J. Am. Chem. Soc. *138*, 7436–7441. https://doi.org/10.1021/jacs.6b04069.
94. McClain, E.J., Monos, T.M., Mori, M., Beatty, J.W., and Stephenson, C.R.J. (2020). Design and Implementation of a Catalytic Electron Donor–Acceptor Complex Platform for Radical Trifluoromethylation and Alkylation. ACS Catal. *10*, 12636–12641. https://doi.org/10.1021/acscatal.0c03837.
95. de Pedro Beato, E., Spinnato, D., Zhou, W., and Melchiorre, P. (2021). A General Organocatalytic System for Electron Donor–Acceptor Complex Photoactivation and Its Use in Radical Processes. J. Am. Chem. Soc. *143*, 12304–12314. https://doi.org/10.1021/jacs.1c05607.
96. Yuan, W., Huang, J., Xu, X., Wang, L., and Tang, X.-Y. (2021). B(C6F5)3-Catalyzed Electron Donor–Acceptor Complex-Mediated Aerobic Sulfenylation of Indoles under Visible-Light Conditions. Org. Lett. *23*, 7139–7143. https://doi.org/10.1021/acs.orglett.1c02553.
97. Zhou, W., Wu, S., and Melchiorre, P. (2022). Tetrachlorophthalimides as Organocatalytic Acceptors for Electron Donor–Acceptor Complex Photoactivation. J. Am. Chem. Soc. *144*, 8914–8919. https://doi.org/10.1021/jacs.2c03546.
98. Troian-Gautier, L., Beauvilliers, E.E., Swords, W.B., and Meyer, G.J. (2016). Redox Active Ion-Paired Excited States Undergo Dynamic

Electron Transfer. J. Am. Chem. Soc. *138*, 16815–16826. https://doi.org/10.1021/jacs.6b11337.

99. Ye, Y., Garrido-Barros, P., Wellauer, J., Cruz, C.M., Lescouëzec, R., Wenger, O.S., Herrera, J.M., and Jiménez, J.-R. (2024). Luminescence and Excited-State Reactivity in a Heteroleptic Tricyanido Fe(III) Complex. J. Am. Chem. Soc. *146*, 954–960. https://doi.org/10.1021/jacs.3c11517.
100. Glaser, F., Schmitz, M., and Kerzig, C. (2023). Coulomb interactions for mediator-enhanced sensitized triplet–triplet annihilation upconversion in solution. Nanoscale *16*, 123–137. https://doi.org/10.1039/D3NR05265F.
101. Singh-Rachford, T.N., and Castellano, F.N. (2010). Photon upconversion based on sensitized triplet–triplet annihilation. Coord. Chem. Rev. *254*, 2560–2573. https://doi.org/10.1016/j.ccr.2010.01.003.
102. Uji, M., Zähringer, T.J.B., Kerzig, C., and Yanai, N. (2023). Visible-to-UV Photon Upconversion: Recent Progress in New Materials and Applications. Angew. Chem. Int. Ed. *62*, e202301506. https://doi.org/10.1002/anie.202301506.
103. Schloemer, T., Narayanan, P., Zhou, Q., Belliveau, E., Seitz, M., and Congreve, D.N. (2023). Nanoengineering Triplet–Triplet Annihilation Upconversion: From Materials to Real-World Applications. ACS Nano *17*, 3259–3288. https://doi.org/10.1021/acsnano.3c00543.
104. Wilke, B.M., and Castellano, F.N. (2013). Photochemical Upconversion: A Physical or Inorganic Chemistry Experiment for Undergraduates Using a Conventional Fluorimeter. J. Chem. *90*, 786–789. https://doi.org/10.1021/ed300142z.
105. Edhborg, F., Olesund, A., and Albinsson, B. (2022). Best practice in determining key photophysical parameters in triplet–triplet annihilation photon upconversion. Photochem. Photobiol. Sci. *21*, 1143–1158. https://doi.org/10.1007/s43630-022-00219-x.
106. Durandin, N.A., Isokuortti, J., Efimov, A., Vuorimaa-Laukkanen, E., Tkachenko, N.V., and Laaksonen, T. (2019). Critical Sensitizer Quality Attributes for Efficient Triplet–Triplet Annihilation Upconversion with Low Power Density Thresholds. J. Phys. Chem. C *123*, 22865–22872. https://doi.org/10.1021/acs.jpcc.9b08026.
107. Murakami, Y., and Kamada, K. (2021). Kinetics of photon upconversion by triplet–triplet annihilation: a comprehensive tutorial. Phys. Chem. Chem. Phys. *23*, 18268–18282. https://doi.org/10.1039/D1CP02654B.
108. Schmitz, M., Bertrams, M. S., Sell, A. C., Glaser, F., & Kerzig, C. (2024). Efficient Energy and Electron Transfer Photocatalysis with a Coulombic Dyad. *Journal of the American Chemical Society*, Advance online publication. https://doi.org/10.1021/jacs.4c08551.
109. Wang, J.-W., Huang, H.-H., Wang, P., Yang, G., Kupfer, S., Huang, Y., Li, Z., Ke, Z., and Ouyang, G. (2022). Co-facial π–π Interaction Expedites Sensitizer-to-Catalyst Electron Transfer for High-Performance CO2 Photoreduction. JACS Au *2*, 1359–1374. https://doi.org/10.1021/jacsau.2c00073.
110. McNaught, A.D., and Wilkinson, A. (1997). Compendium of chemical terminology: IUPAC recommendations. the Gold book.
111. Gehlen, M.H. (2020). The centenary of the Stern-Volmer equation of fluorescence quenching: From the single line plot to the SV quenching map. J. Photoch. Photobio. C *42*, 100338. https://doi.org/10.1016/j.jphotochemrev.2019.100338.
112. Stern, O., and Volmer, M. (1919). Über die Abklingungszit der Fluoreszenz. Phyzik. Z. *20*, 183–188.
113. De Kreijger, S., Gillard, M., Elias, B., and Troian-Gautier, L. (2024). Spectroscopic Techniques to Unravel Mechanistic Details in Light-Induced Transformations and Photoredox Catalysis. ChemCatChem *16*, e202301100. https://doi.org/10.1002/cctc.202301100.
114. Arias-Rotondo, D.M., and McCusker, J.K. (2016). The photophysics of photoredox catalysis: a roadmap for catalyst design. Chem. Soc. Rev. *45*, 5803–5820. https://doi.org/10.1039/C6CS00526H.
115. Till, N.A., Tian, L., Dong, Z., Scholes, G.D., and MacMillan, D.W.C. (2020). Mechanistic Analysis of Metallaphotoredox C–N Coupling: Photocatalysis Initiates and Perpetuates Ni(I)/Ni(III) Coupling Activity. J. Am. Chem. Soc. *142*, 15830–15841. https://doi.org/10.1021/jacs.0c05901.
116. Chan, A.Y., Perry, I.B., Bissonnette, N.B., Buksh, B.F., Edwards, G.A., Frye, L.I., Garry, O.L., Lavagnino, M.N., Li, B.X., Liang, Y., et al. (2022). Metallaphotoredox: The Merger of Photoredox and Transition Metal Catalysis. Chem. Rev. *122*, 1485–1542. https://doi.org/10.1021/acs.chemrev.1c00383.
117. DiLuzio, S., Kannadi Valloli, L., Kudisch, M., Chambers, D.T., Rumbles, G., Reid, O.G., Bird, M.J., and Sayre, H.J. (2024). Reconceptualizing the IrIII Role in Metallaphotoredox Catalysis: From Strong Photooxidant to Potent Energy Donor. ACS Catal. *14*, 11378–11388. https://doi.org/10.1021/acscatal.4c03350.
118. van der Meer, B.W. (2013). Förster Theory. In FRET – Förster Resonance Energy Transfer, pp. 23–62. https://doi.org/10.1002/9783527656028.ch03.
119. Dexter, D.L. (1953). A Theory of Sensitized Luminescence in Solids. J. Chem. Phys. *21*, 836–850. https://doi.org/10.1063/1.1699044.
120. Wigner, E. (1927). Über die Erhaltungssätze in der Quantenmechanik. Nachrichten von der Gesellschaft der Wissenschaften zu Göttingen. Mathematisch-Physikalische Klasse *1927*, 375–381.
121. Braslavsky, S.E. (2007). Glossary of terms used in photochemistry, 3rd edition (IUPAC Recommendations 2006). Pure Appl. Chem. *79*, 293–465. https://doi.org/10.1351/pac200779030293.
122. Schweitzer, C., and Schmidt, R. (2003). Physical Mechanisms of Generation and Deactivation of Singlet Oxygen. Chem. Rev. *103*, 1685–1757. https://doi.org/10.1021/cr010371d.
123. Han, J., Jiang, Y., Obolda, A., Duan, P., Li, F., and Liu, M. (2017). Doublet–Triplet Energy Transfer-Dominated Photon Upconversion. J. Phys. Chem. Lett. *8*, 5865–5870. https://doi.org/10.1021/acs.jpclett.7b02677.
124. Wei, Y., An, K., Xu, X., Ye, Z., Yin, X., Cao, X., and Yang, C. (2024). Π-Radical Photosensitizer for Highly Efficient and Stable Near-Infrared Photon Upconversion. Adv. Opt. Mater. *12*, 2301134. https://doi.org/10.1002/adom.202301134.
125. Wang, C., Reichenauer, F., Kitzmann, W.R., Kerzig, C., Heinze, K., and Resch-Genger, U. (2022). Efficient Triplet-Triplet Annihilation Upconversion Sensitized by a Chromium(III) Complex via an Underexplored Energy Transfer Mechanism. Angew. Chem. Int. Ed. *61*, e202202238. https://doi.org/10.1002/anie.202202238.
126. Naimovičius, L., Bharmoria, P., and Moth-Poulsen, K. (2023). Triplet–triplet annihilation mediated photon upconversion solar energy systems. Mater. Chem. Front. *7*, 2297–2315. https://doi.org/10.1039/D3QM00069A.
127. Bossanyi, D.G., Sasaki, Y., Wang, S., Chekulaev, D., Kimizuka, N., Yanai, N., and Clark, J. (2021). Spin Statistics for Triplet–Triplet Annihilation Upconversion: Exchange Coupling, Intermolecular Orientation, and Reverse Intersystem Crossing. JACS Au *1*, 2188–2201. https://doi.org/10.1021/jacsau.1c00322.
128. Neveselý, T., Wienhold, M., Molloy, J.J., and Gilmour, R. (2022). Advances in the E → Z Isomerization of Alkenes Using Small Molecule Photocatalysts. Chem. Rev. *122*, 2650–2694. https://doi.org/10.1021/acs.chemrev.1c00324.
129. Chatterjee, A., and König, B. (2019). Birch-Type Photoreduction of Arenes and Heteroarenes by Sensitized Electron Transfer. Angew. Chem. Int. Ed. *58*, 14289–14294. https://doi.org/10.1002/anie.201905485.
130. Dutta, S., Erchinger, J.E., Strieth-Kalthoff, F., Kleinmans, R., and Glorius, F. (2024). Energy transfer photocatalysis: exciting modes of reactivity. Chem. Soc. Rev. *53*, 1068–1089. https://doi.org/10.1039/D3CS00190C.
131. Zhou, Q.-Q., Zou, Y.-Q., Lu, L.-Q., and Xiao, W.-J. (2019). Visible-Light-Induced Organic Photochemical Reactions through Energy-Transfer Pathways. Angew. Chem. Int. Ed. *58*, 1586–1604. https://doi.org/10.1002/anie.201803102.
132. Seo, S.E., Choe, H.-S., Cho, H., Kim, H.-i., Kim, J.-H., and Kwon, O.S. (2022). Recent advances in materials for and applications of triplet–triplet annihilation-based upconversion. J. Mater. Chem. C *10*, 4483–4496. https://doi.org/10.1039/D1TC03551G.

133. Kalyanasundaram, K. (1982). Photophysics, photochemistry and solar energy conversion with tris(bipyridyl)ruthenium(II) and its analogues. Coord. Chem. Rev. *46*, 159–244. https://doi.org/10.1016/0010-8545(82)85003-0.

134. Rehm, D., and Weller, A. (1969). Kinetik und Mechanismus der Elektronübertragung bei der Fluoreszenzlöschung in Acetonitril. Ber. Bunsenges. Phys. Chem. *73*, 834–839. https://doi.org/10.1002/bbpc.19690730818.

135. Rehm, D., and Weller, A. (1970). Kinetics of fluorescence quenching by electron and H-atom transfer. Isr. J. Chem. *8*, 259–271.

136. Meroni, D., Monguzzi, A., and Meinardi, F. (2020). Photon upconversion in multicomponent systems: Role of back energy transfer. J. Chem. Phys. *153*, 114302. https://doi.org/10.1063/5.0021253.

137. Marcus, R.A. (1956). On the Theory of Oxidation-Reduction Reactions Involving Electron Transfer. I. J. Chem. Phys. *24*, 966–978. https://doi.org/10.1063/1.1742723.

138. Migliore, A., Polizzi, N.F., Therien, M.J., and Beratan, D.N. (2014). Biochemistry and Theory of Proton-Coupled Electron Transfer. Chem. Rev. *114*, 3381–3465. https://doi.org/10.1021/cr4006654.

139. Turró, C., Zaleski, J.M., Karabatsos, Y.M., and Nocera, D.G. (1996). Bimolecular Electron Transfer in the Marcus Inverted Region. J. Am. Chem. Soc. *118*, 6060–6067. https://doi.org/10.1021/ja960575p.

140. Piechota, E.J., and Meyer, G.J. (2019). Introduction to Electron Transfer: Theoretical Foundations and Pedagogical Examples. J. Chem. *96*, 2450–2466. https://doi.org/10.1021/acs.jchemed.9b00489.

141. Marcus, R.A., and Sutin, N. (1985). Electron transfers in chemistry and biology. BBA-Bioenergetics *811*, 265–322. https://doi.org/10.1016/0304-4173(85)90014-X.

142. Miller, J.R., Calcaterra, L.T., and Closs, G.L. (1984). Intramolecular long-distance electron transfer in radical anions. The effects of free energy and solvent on the reaction rates. J. Am. Chem. Soc. *106*, 3047–3049. https://doi.org/10.1021/ja00322a058.

143. Rosspeintner, A., Angulo, G., and Vauthey, E. (2014). Bimolecular Photoinduced Electron Transfer Beyond the Diffusion Limit: The Rehm–Weller Experiment Revisited with Femtosecond Time Resolution. J. Am. Chem. Soc. *136*, 2026–2032. https://doi.org/10.1021/ja4118279.

144. Eriksen, J., Joergensen, K.A., Linderberg, J., and Lund, H. (1984). Electron-transfer fluorescence quenching of radical ions. Experimental work and theoretical calculations. J. Am. Chem. Soc. *106*, 5083–5087. https://doi.org/10.1021/ja00330a008.

145. Gould, I.R., Ege, D., Mattes, S.L., and Farid, S. (1987). Return electron transfer within geminate radical ion pairs. Observation of the Marcus inverted region. J. Am. Chem. Soc. *109*, 3794–3796. https://doi.org/10.1021/ja00246a055.

146. Juneau, A., Hope, T.O., Malenfant, J., Mesko, M., McNeill, J., and Frenette, M. (2022). Methods to Predict Potential Reagents in Iridium-Based Photoredox Catalysis Calibrated with Stern–Volmer Quenching Rate Constants. ACS Catal. *12*, 2348–2356. https://doi.org/10.1021/acscatal.1c04740.

147. (2019). Rehm–Weller Equation (International Union of Pure and Applied Chemistry (IUPAC)). https://doi.org/10.1351/goldbook.RT07472.

148. Stubbe, J., Nocera, D.G., Yee, C.S., and Chang, M.C.Y. (2003). Radical Initiation in the Class I Ribonucleotide Reductase: Long-Range Proton-Coupled Electron Transfer? Chem. Rev. *103*, 2167–2201. https://doi.org/10.1021/cr020421u.

149. Agmon, N., and Levine, R.D. (1977). Energy, entropy and the reaction coordinate: thermodynamic-like relations in chemical kinetics. Chem. Phys. Lett. *52*, 197–201. https://doi.org/10.1016/0009-2614(77)80523-X.

150. Scandola, F., and Balzani, V. (1979). Free-energy relationships for electron-transfer processes. J. Am. Chem. Soc. *101*, 6140–6142. https://doi.org/10.1021/ja00514a057.

151. Eriksen, J., Lund, H., Nyvad, A.I., Yamato, T., Mitchell, R.H., Dingle, T.W., Williams, R.V., and Mahedevan, R. (1983). Electron-transfer fluorescence quenching of radical ions. Acta Chem. Scand. *37b*, 459–466.

152. Zeman, C.J., 4th, Kim, S., Zhang, F., and Schanze, K.S. (2020). Direct Observation of the Reduction of Aryl Halides by a Photoexcited Perylene Diimide Radical Anion. J. Am. Chem. Soc. *142*, 2204–2207. https://doi.org/10.1021/jacs.9b13027.

153. Sau, S.C., Schmitz, M., Burdenski, C., Baumert, M., Antoni, P.W., Kerzig, C., and Hansmann, M.M. (2024). Dicationic Acridinium/Carbene Hybrids as Strongly Oxidizing Photocatalysts. J. Am. Chem. Soc. *146*, 3416–3426. https://doi.org/10.1021/jacs.3c12766.

154. Bürgin, T.H., Glaser, F., and Wenger, O.S. (2022). Shedding Light on the Oxidizing Properties of Spin-Flip Excited States in a CrIII Polypyridine Complex and Their Use in Photoredox Catalysis. J. Am. Chem. Soc. *144*, 14181–14194. https://doi.org/10.1021/jacs.2c04465.

155. Sandros, K., Haglid, F., Ryhage, R., Ryhage, R., and Stevens, R. (1964). Transfer of Triplet State Energy in Fluid Solutions. III. Reversible Energy Transfer. Acta Chem. Scand. *18*, 2355–2374.

156. Herkstroeter, W.G., and Hammond, G.S. (1966). Mechanisms of Photochemical Reactions in Solution. XXXIX.1 Study of Energy Transfer by Kinetic Spectrophotometry. J. Am. Chem. Soc. *88*, 4769–4777. https://doi.org/10.1021/ja00973a001.

157. Balzani, V., Bolletta, F., and Scandola, F. (1980). Vertical and "nonvertical" energy transfer processes. A general classical treatment. J. Am. Chem. Soc. *102*, 2152–2163. https://doi.org/10.1021/ja00527a002.

158. Zähringer, T.J.B., Wienhold, M., Gilmour, R., and Kerzig, C. (2023). Direct Observation of Triplet States in the Isomerization of Alkenylboronates by Energy Transfer Catalysis. J. Am. Chem. Soc. *145*, 21576–21586. https://doi.org/10.1021/jacs.3c07678.

159. Kornfeld, G., Farkas, L., and Rabinowitsch, E. (1934). General discussion. Trans. Faraday Soc. *30*, 130–131. https://doi.org/10.1039/TF9343000130.

160. Franck, J., and Rabinowitsch, E. (1934). Some remarks about free radicals and the photochemistry of solutions. Trans. Faraday Soc. *30*, 120–130. https://doi.org/10.1039/TF9343000120.

161. Lyon, R.K., and Levy, D.H. (1961). Demonstration of the "Cage" Effect. J. Am. Chem. Soc. *83*, 4290. https://doi.org/10.1021/ja01481a047.

162. Jayanthi, S.S., and Ramamurthy, P. (1999). Photoinduced electron transfer reactions of 2,4,6 triphenylpyrylium: solvent effect and charge-shift type of systems. Phys. Chem. Chem. Phys. *1*, 4751–4757.

163. Aydogan, A., Bangle, R.E., Cadranel, A., Turlington, M.D., Conroy, D.T., Cauët, E., Singleton, M.L., Meyer, G.J., Sampaio, R.N., Elias, B., and Troian-Gautier, L. (2021). Accessing Photoredox Transformations with an Iron(III) Photosensitizer and Green Light. J. Am. Chem. Soc. *143*, 15661–15673. https://doi.org/10.1021/jacs.1c06081.

164. Wolff, H.-J., Bürßner, D., and Steiner, U.E. (1995). Spin-orbit coupling controlled spin chemistry of $Ru(bpy)_3^{2+}$ photooxidation: Detection of strong viscosity dependence of in-cage backward electron transfer rate. Pure Appl. Chem. *67*, 167–174.

165. Meidlar, K., and Das, P.K. (1982). Tris(2,2'-bipyridine)ruthenium(II)-Sensitized Photooxidation of Phenols. Environmental Effects on Electron Transfer Yields and Kinetics. J. Am. Chem. Soc. *104*, 7462–7469.

166. Ohno, T., and Lichtin, N.N. (1980). Electron Transfer in the Quenching of Triplet Methylene Blue by Complexes of Iron(II). J. Am. Chem. Soc. *102*, 4636–4643.

167. Sun, H., Neshvad, G., and Hoffman, M.Z. (2006). Energy Gap Dependence of the Efficiency of Charge Separation upon the Sacrificial Reductive Quenching of the Excited States of Ru(II)-Diimine Photosensitizers in Aqueous Solution. Mol. Cryst. Liq. Cryst. *194*, 141–150. https://doi.org/10.1080/00268949108041159.

168. DiLuzio, S., Connell, T.U., Mdluli, V., Kowalewski, J.F., and Bernhard, S. (2022). Understanding Ir(III) Photocatalyst Structure-Activity Relationships: A Highly Parallelized Study of Light-Driven Metal Reduction

Processes. J. Am. Chem. Soc. *144*, 1431–1444. https://doi.org/10.1021/jacs.1c12059.

169. Hoffman, M.Z. (1988). Cage Escape Yields from the Quenching of $^*Ru(bpy)_3^{2+}$ by Methylviologen in Aqueous Solution. J. Phys. Chem. *92*, 3458–3464. https://doi.org/10.1021/j100323a029.
170. Gibbons, D.J., Farawar, A., Mazzella, P., Leroy-Lhez, S., and Williams, R.M. (2020). Making triplets from photo-generated charges: observations, mechanisms and theory. Photochem. Photobiol. Sci. *19*, 136–158. https://doi.org/10.1039/c9pp00399a.
171. Olmsted, J., and Meyer, T.J. (1987). Factors affecting cage escape yields following electron-transfer quenching. J. Phys. Chem. *91*, 1649–1655. https://doi.org/10.1021/j100290a071.
172. Kikuchi, K., Hoshi, M., Niwa, T., Takahashi, Y., and Miyashi, T. (1991). Heavy-atom effects on the excited singlet-state electron-transfer reaction. J. Phys. Chem. *95*, 38–42.
173. Kalyanasundaram, K., and Neumann-Spallart, M. (1982). Influence of added salts on the cage escape yields in the photoredox quenching of $Ru(bpy)_2^{+3}$ excited states. Chem. Phys. Lett. *88*, 7–12.
174. Aydogan, A., Bangle, R.E., De Kreijger, S., Dickenson, J.C., Singleton, M.L., Cauët, E., Cadranel, A., Meyer, G.J., Elias, B., Sampaio, R.N., and Troian-Gautier, L. (2021). Mechanistic investigation of a visible light mediated dehalogenation/cyclisation reaction using iron(iii), iridium(iii) and ruthenium(ii) photosensitizers. Catal. Sci. Technol. *11*, 8037–8051. https://doi.org/10.1039/D1CY01771C.
175. Wang, C., Li, H., Bürgin, T.H., and Wenger, O.S. (2024). Cage escape governs photoredox reaction rates and quantum yields. Nat. Chem. https://doi.org/10.1038/s41557-024-01482-4.
176. Goodwin, M.J., Dickenson, J.C., Ripak, A., Deetz, A.M., McCarthy, J.S., Meyer, G.J., and Troian-Gautier, L. (2024). Factors that Impact Photochemical Cage Escape Yields. Chem. Rev. *124*, 7379–7464. https://doi.org/10.1021/acs.chemrev.3c00930.
177. Ripak, A., De Kreijger, S., Sampaio, R.N., Vincent, C.A., Cauët, É., Jabin, I., Tambar, U.K., Elias, B., and Troian-Gautier, L. (2023). Photosensitized activation of diazonium derivatives for C–B bond formation. Chem Catal. *3*, 100490. https://doi.org/10.1016/j.checat.2022.100490.
178. Kurtz, D.A., and Dempsey, J.L. (2019). Proton-Coupled Electron Transfer Kinetics for the Photoinduced Generation of a Cobalt(III)-Hydride Complex. Inorg. Chem. *58*, 16510–16517. https://doi.org/10.1021/acs.inorgchem.9b02445.
179. DiMarco, B.N., O'Donnell, R.M., and Meyer, G.J. (2015). Cation-Dependent Charge Recombination to Organic Mediators in Dye-Sensitized Solar Cells. J. Phys. Chem. C *119*, 21599–21604. https://doi.org/10.1021/acs.jpcc.5b07342.
180. Wehlin, S.A.M., Troian-Gautier, L., Li, G., and Meyer, G.J. (2017). Chloride Oxidation by Ruthenium Excited-States in Solution. J. Am. Chem. Soc. *139*, 12903–12906. https://doi.org/10.1021/jacs.7b06762.
181. Glaser, F., Kerzig, C., and Wenger, O.S. (2021). Sensitization-initiated electron transfer via upconversion: mechanism and photocatalytic applications. Chem. Sci. *12*, 9922–9933. https://doi.org/10.1039/D1SC02085D.
182. Sreenath, K., Thomas, T.G., and Gopidas, K.R. (2011). Cu(II) Mediated Generation and Spectroscopic Study of the Tris(4-anisyl)amine Radical Cation and Dication. Unusually Shielded Chemical Shifts in the Dication. Org. Lett. *13*, 1134–1137. https://doi.org/10.1021/ol103167m.
183. DiMarco, B.N., Troian-Gautier, L., Sampaio, R.N., and Meyer, G.J. (2018). Dye-sensitized electron transfer from TiO2 to oxidized triphenylamines that follows first-order kinetics. Chem. Sci. *9*, 940–949. https://doi.org/10.1039/C7SC03839A.
184. Yoshimura, A., Hoffman, M.Z., and Sun, H. (1993). An evaluation of the excited state absorption spectrum of Ru(bpy)32+ in aqueous and acetonitrile solutions. J. Photochem. Photobiol., A *70*, 29–33. https://doi.org/10.1016/1010-6030(93)80005-T.
185. Goez, M., von Ramin-Marro, D., Othman Musa, M.H., and Schiewek, M. (2004). Photoionization of [Ru(bpy)3]2+: A Catalytic Cycle with Water as Sacrificial Donor. J. Phys. Chem. A *108*, 1090–1100. https://doi.org/10.1021/jp036790r.
186. Müller, P., and Brettel, K. (2012). [Ru(bpy)3]2+ as a reference in transient absorption spectroscopy: differential absorption coefficients for formation of the long-lived 3MLCT excited state. Photochem. Photobiol. Sci. *11*, 632–636. https://doi.org/10.1039/C2PP05333K.
187. Ripak, A., De Kreijger, S., Elias, B., and Troian-Gautier, L. (2023). A protocol for determining cage-escape yields using nanosecond transient absorption spectroscopy. STAR Protoc. *4*, 102312. https://doi.org/10.1016/j.xpro.2023.102312.
188. De Kreijger, S., Elias, B., and Troian-Gautier, L. (2023). Chloride, Bromide, and Iodide Photooxidation in Acetonitrile/Water Mixtures Using Binuclear Iridium(III) Photosensitizers. Inorg. Chem. *62*, 16196–16202. https://doi.org/10.1021/acs.inorgchem.3c02648.
189. Stevenson, B.G., Spielvogel, E.H., Loiaconi, E.A., Wambua, V.M., Nakhamiyayev, R.V., and Swierk, J.R. (2021). Mechanistic Investigations of an α-Aminoarylation Photoredox Reaction. J. Am. Chem. Soc. *143*, 8878–8885. https://doi.org/10.1021/jacs.1c03693.
190. Kjær, K.S., Kaul, N., Prakash, O., Chábera, P., Rosemann, N.W., Honarfar, A., Gordivska, O., Fredin, L.A., Bergquist, K.-E., Häggström, L., et al. (2019). Luminescence and reactivity of a charge-transfer excited iron complex with nanosecond lifetime. Science *363*, 249–253. https://doi.org/10.1126/science.aau7160.
191. Ripak, A., Vega Salgado, A.K., Valverde, D., Cristofaro, S., de Gary, A., Olivier, Y., Elias, B., and Troian-Gautier, L. (2024). Factors Controlling Cage Escape Yields of Closed- and Open-Shell Metal Complexes in Bimolecular Photoinduced Electron Transfer. J. Am. Chem. Soc. *146*, 22818–22828. https://doi.org/10.1021/jacs.4c08158.
192. Glaser, F., Kerzig, C., and Wenger, O.S. (2020). Multi-Photon Excitation in Photoredox Catalysis: Concepts, Applications, Methods. Angew. Chem. Int. Ed. *59*, 10266–10284. https://doi.org/10.1002/anie.201915762.
193. Kerzig, C., and Wenger, O.S. (2019). Reactivity control of a photocatalytic system by changing the light intensity. Chem. Sci. *10*, 11023–11029. https://doi.org/10.1039/C9SC04584H.
194. Pitre, S.P., McTiernan, C.D., Vine, W., DiPucchio, R., Grenier, M., and Scaiano, J.C. (2015). Visible-Light Actinometry and Intermittent Illumination as Convenient Tools to Study Ru(bpy)3Cl2 Mediated Photoredox Transformations. Sci. Rep. *5*, 16397. https://doi.org/10.1038/srep16397.
195. Kuhn, H.J., Braslavsky, S.E., and Schmidt, R. (2004). Chemical actinometry (IUPAC Technical Report). Pure Appl. Chem. *76*, 2105–2146. https://doi.org/10.1351/pac200476122105.
196. El Achi, N., Bakkour, Y., Chausset-Boissarie, L., Penhoat, M., and Rolando, C. (2017). Rapid and facile chemical actinometric protocol for photo-microfluidic systems using azobenzene and NMR spectroscopy. RSC Adv. *7*, 29815–29820. https://doi.org/10.1039/C7RA01237C.
197. Lehnherr, D., Ji, Y., Neel, A.J., Cohen, R.D., Brunskill, A.P.J., Yang, J., and Reibarkh, M. (2018). Discovery of a Photoinduced Dark Catalytic Cycle Using in Situ LED-NMR Spectroscopy. J. Am. Chem. Soc. *140*, 13843–13853. https://doi.org/10.1021/jacs.8b08596.
198. Ji, Y., DiRocco, D.A., Kind, J., Thiele, C.M., Gschwind, R.M., and Reibarkh, M. (2019). LED-Illuminated NMR Spectroscopy: A Practical Tool for Mechanistic Studies of Photochemical Reactions. ChemPhotoChem *3*, 984–992. https://doi.org/10.1002/cptc.201900109.
199. Skubi, K.L., Swords, W.B., Hofstetter, H., and Yoon, T.P. (2020). LED-NMR Monitoring of an Enantioselective Catalytic [2+2] Photocycloaddition. ChemPhotoChem *4*, 685–690. https://doi.org/10.1002/cptc.202000094.
200. Picchetti, P., DiMarco, B.N., Travaglini, L., Zhang, Y., Ortega-Liebana, M.C., and De Cola, L. (2020). Breaking with Light: Stimuli-Responsive Mesoporous Organosilica Particles. Chem. Mater. *32*, 392–399. https://doi.org/10.1021/acs.chemmater.9b03937.
201. Feuerstein, T.J., Müller, R., Barner-Kowollik, C., and Roesky, P.W. (2019). Investigating the Photochemistry of Spiropyran Metal Complexes

with Online LED-NMR. Inorg. Chem. *58*, 15479–15486. https://doi.org/10.1021/acs.inorgchem.9b02547.

202. Ji, Y., DiRocco, D.A., Hong, C.M., Wismer, M.K., and Reibarkh, M. (2018). Facile Quantum Yield Determination via NMR Actinometry. Org. Lett. *20*, 2156–2159. https://doi.org/10.1021/acs.orglett.8b00391.

203. Sakakibara, Y., and Murakami, K. (2022). Switchable Divergent Synthesis Using Photocatalysis. ACS Catal. *12*, 1857–1878. https://doi.org/10.1021/acscatal.1c05318.

204. Cañellas, S., Nuño, M., and Speckmeier, E. (2024). Improving reproducibility of photocatalytic reactions—how to facilitate broad application of new methods. Nat. Commun. *15*, 307. https://doi.org/10.1038/s41467-023-44362-0.

205. Svejstrup, T.D., Chatterjee, A., Schekin, D., Wagner, T., Zach, J., Johansson, M.J., Bergonzini, G., and König, B. (2021). Effects of Light Intensity and Reaction Temperature on Photoreactions in Commercial Photoreactors. ChemPhotoChem *5*, 808–814. https://doi.org/10.1002/cptc.202100059.

206. Ziegenbalg, D., Pannwitz, A., Rau, S., Dietzek-Ivanšić, B., and Streb, C. (2022). Comparative Evaluation of Light-Driven Catalysis: A Framework for Standardized Reporting of Data. Angew. Chem. Int. Ed. *61*, e202114106. https://doi.org/10.1002/anie.202114106.

207. Jacob, C., Baguia, H., Dubart, A., Oger, S., Thilmany, P., Beaudelot, J., Deldaele, C., Peruško, S., Landrain, Y., Michelet, B., et al. (2022). A general synthesis of azetidines by copper-catalysed photoinduced anti-Baldwin radical cyclization of ynamides. Nat. Commun. *13*, 560.

208. Bryden, M.A., Crovini, E., Comerford, T., Studer, A., and Zysman-Colman, E. (2024). Organic Donor–Acceptor Thermally Activated Delayed Fluorescence Photocatalysts in the Photoinduced Dehalogenation of Aryl Halides. Angew. Chem. Int. Ed. n/a *63*, e202405081. https://doi.org/10.1002/anie.202405081.

209. Sau, A., Pompetti, N.F., Green, A.R., Popescu, M.V., Paton, R.S., Miyake, G.M., and Damrauer, N.H. (2024). Mechanistic Investigation of a Photocatalyst Model Reveals Function by Perylene-Like Closed Shell Super-Photoreductant Capable of Reducing Unactivated Arenes. ACS Catal. *14*, 2252–2263. https://doi.org/10.1021/acscatal.3c05386.

210. Cole, J.P., Chen, D.-F., Kudisch, M., Pearson, R.M., Lim, C.-H., and Miyake, G.M. (2020). Organocatalyzed Birch Reduction Driven by Visible Light. J. Am. Chem. Soc. *142*, 13573–13581. https://doi.org/10.1021/jacs.0c05899.

211. Žurauskas, J., Boháčová, S., Wu, S., Butera, V., Schmid, S., Domański, M., Slanina, T., and Barham, J.P. (2023). Electron-Poor Acridones and Acridiniums as Super Photooxidants in Molecular Photoelectrochemistry by Unusual Mechanisms. Angew. Chem. Int. Ed. *62*, e202307550. https://doi.org/10.1002/anie.202307550.

212. Pelosin, P., Gil-Sepulcre, M., Garrido-Barros, P., Moonshiram, D., Benet-Buchholz, J., Gimbert-Suriñach, C., and Llobet, A. (2020). Analysis of the Active Species Responsible for Water Oxidation Using a Pentanuclear Fe Complex. iScience *23*, 101378. https://doi.org/10.1016/j.isci.2020.101378.